university of groningen / faculty of science and engineering

The 3D Printing of a Bio-Inspired Flow Sensor System

Bachelor's Thesis for Biomedical Engineering

Thom van der Honing (S4495012)
Under the supervision of Prof. Dr. A.G.P. Kottapalli and Dr. A.M. Kamat

Version 1
June 25, 2023

Abstract

In this study a sensor system is developed inspired by the morphology of seal whiskers, which are known to suppress vortex induced vibrations. The main objective of this study is to design and make a functioning sensor by using only FDM 3D printing techniques. To achieve this design, first a guideline is developed on how to print with flexible materials. The printed sensor was tested by subjecting three different whiskers to a series of flow velocities. The measured output of the sensor matches the visual observation done during the experiment, proving that it is possible to successfully print a sensor. The output of the sensor also proves that the seal whisker morphology can indeed suppress vortex induced vibrations. While the sensor provides consistent output, the repeatability of the printed sensor gauges is less than optimal, which is due to printing accuracy and inconsistencies in the filament.

Contents

1. Introduction **4**
2. Sensor Design **5**
2.1 - Design Considerations 5
2.2 - Final Prototype 5
2.3 - Initial Testing 6
2.4 - Data Acquisition 7
3. Experimental Section **8**
3.1 - Experimental Setup 8
3.2 - Data Processing 8
4. Results **10**
4.1 - Temporal Analysis of Whisker Vibration 10
4.2 - Frequency Analysis of Whisker Vibration 10
5. Conclusion **13**
6. Discussion **13**
6.1 - Quality of Printing, Sensor Wiring and Experimental Design 13
6.2 - Time Constraints 13
7. Future Work **14**
Bibliography **15**
Appendices **18**
A. - Printing with Flexible Filaments 18
B. - Technical Drawings 20
C. - Raw Data 22
D. - Graphs 24

1. Introduction

Normally, when a flow passes an object, turbulent eddy currents form at the edges. These vortices introduce lift- and drag forces to the object, thus pushing the object to a direction perpendicular to the flow. The forces change dynamically causing a repetitive change in direction. This vibration is called a vortex-induced vibration (VIV).[1] The shedding of the vortices left by an object often occurs in a repetitive fashion, creating a Karman vortex street in its wake. The vibrissae of phocid seals are known to suppress those VIVs due to the undulating elliptical helix morphology found on the whiskers.[2][3] During a normal flow, which is the constant swimming of the seal through water, almost no vibrations occur. However, when the seal swims through the wake of another object, the whiskers will vibrate in the surrounding vortices. In the study of Zheng et al. (2022a), where a micro electromechanical system (MEMS) sensor was made using the morphology of the seal whisker, the whisker appeared to be vibrating two-to-ten times more heavily when in the wake of an object.[4] An increase of this much results in a high signal-to-noise ratio. These vibrations, when caused by the wake of another object, are called wake-induced vibrations (WIV). Seal whiskers are elliptical in cross-section, and therefore have a major axis and a minor axis. The angle that the whisker makes with respect to the flow influences the sensitivity of the sensor. According to Zheng et al. (2022), the whisker angle is limited to 0-30 or 150-180 degrees to ensure the smallest VIV induced noise, where a zero-degree orientation implies that the minor axis of the ellipse is pointing towards the flow.[4]

The development of 3D printed sensor systems is an active field in current research. Multiple papers have been published in recent years combining additive manufacturing techniques to create working and reproducible strain sensors. Inkjet printing has been used multiple times to make strain gauges.[6,7] As an example, Agarwala et al. (2017) combined inkjet printing with fused deposition modelling (FDM) techniques to print silver-filled microchannels with a diameter of 500 micrometres, to create working strain gauges.[9] And Yan et al. (2023) explained the use of self healing PDMS in combination with the injection of carbon nanotubes to create piezo resistive strain sensors.[9] However, this combines two different printing techniques, whereas in other studies, single 3D printing techniques were used to make a working sensor. Georgopoulou et al. (2023) used SLA techniques to print a piezoresistive sensor using a self-mixed conductive rubber.[10] The material was homogeneously mixed and therefore the sensors were consistent in their conductivity. The sensor was printed in order of centimetres, where smaller resolution could be achieved. In the article written by Maurizi et al. (2019), a MEMS scale strain gauge was produced with an FDM printer, using a conductive polylactic acid (PLA) filament as sensing element.[11] In these articles however, the use of the strain gauges have only been applied to single cantilever setups.

This study aims to answer two research questions: “How can an FDM printer produce a functional sensor system based on strain gauges?” and “How accurate are the measurements that are performed with an FDM printed sensor system?”. To answer these questions, a bio-inspired flow sensor system is developed. The sensor utilises FDM 3D printing techniques to achieve sensing capabilities in both the X and Y direction, using a commercially available piezoresistive thermoplastic polyurethane (TPU) filament and other materials. A key advantage of this study is the low production costs of a full sensor system, while allowing to measure a sensor output in multiple directions, therefore providing information about the effect of VIVs on both the X and Y direction. This makes the sensor suitable for wake tracking sensing.

This study is subdivided in several chapters, each addressing a specific aspect of the research. Chapter 2 of this study focusses on the sensor design. In chapter 3, the experimental setup is discussed, outlining the methodology used in the measurement. The findings from these measurements are presented in chapter 4, where the results are analysed. Chapter 5 provides a conclusion to this research, giving answer to the research questions. In chapter 6, an in-depth discussion of this study is provided, stating the limitations of the study. Finally, chapter 7 concludes this research by outlining potential improvements to this sensor system and other possible future studies.

2. Sensor Design

2.1 - Design Considerations

Throughout the iterative design process, the sensor base has seen multiple precursor versions. Initially PLA has been considered as a base material, but its elastic properties proved to be less desirable compared to TPU, resulting in the transition to Ulitmaker's TPU 95A filament. To optimise the sensor design, multiple different layer counts were explored in order to find the optimal thickness, as well as diverse sizes and lengths were used for both the strain gauges and the sensor base itself. As part of the design exploration, even an approach was considered where the strain gauges were printed directly onto the whisker. This design concept was discarded rather quickly due to its limited feasibility. Each of these design iterations contributed to the improvement of the overall model, ultimately leading to the final prototype.

2.2 - Final Prototype

The sensor base used in this study is designed to have four membranes with a 200 µm thickness, composing of Ultimaker's TPU 95A filament. The membranes are oriented 90 degrees apart, thus forming a plus-sign. The membranes are surrounded with a 400 µm thick ring connecting the end of the membranes together. On top of the membranes, the strain gauges are printed using the NinjaTek EEL filament, which is a TPU based piezoresistive filament.[12] These resistors are 400 µm in thickness. The whole sensor is printed with one FDM printer, allowing the strain gauges to be partially integrated into the membrane. In the centre of the base an adapter containing a square hole of 5.00 mm by 5.00 mm by 6.00 mm is designed to allow for a same sized cuboid to be inserted. This design is fully 3D printed using an Ultimaker S5 FDM printer. The printed sensor can be seen in Figure 1.A. The sensor base is flexible and elastic because of the material properties of TPU. According to the manufacturer, the NinjaTek EEL material can be elongated up to 355% without breaking.[12] For the tightening of the membrane, the sensor base is placed inside a custom made clamp. This ensures that all the movements of the whisker will cause strain on the sensors, while keeping the outer ring stable. The technical drawings of the final sensor base and corresponding clamp are included in the appendix B, while the CAD-files are attached to this report in the Google Drive.

The whisker used in this experiment is a modified version of “Grey seal whisker V”, taken from the “supplementary information S1” folder, attached to the article by Zheng et al. (2022b).[5] The whisker was scaled up to 830% of the original size, and then trimmed to a length of 130 mm, taking the most straight section of the whisker. To the lower end of the whisker, a 5.00 mm by 5.00 mm by 6.00 mm cuboid is attached to allow for integrating with the sensor base. To compare the seal whisker's effectiveness in reducing VIV, a simple 10.00 mm diameter, 130.00 mm long cylinder is constructed, to which the same cuboid is attached. All the designs were made using the CAD software SOLIDWORKS (Dassault Systèmes).

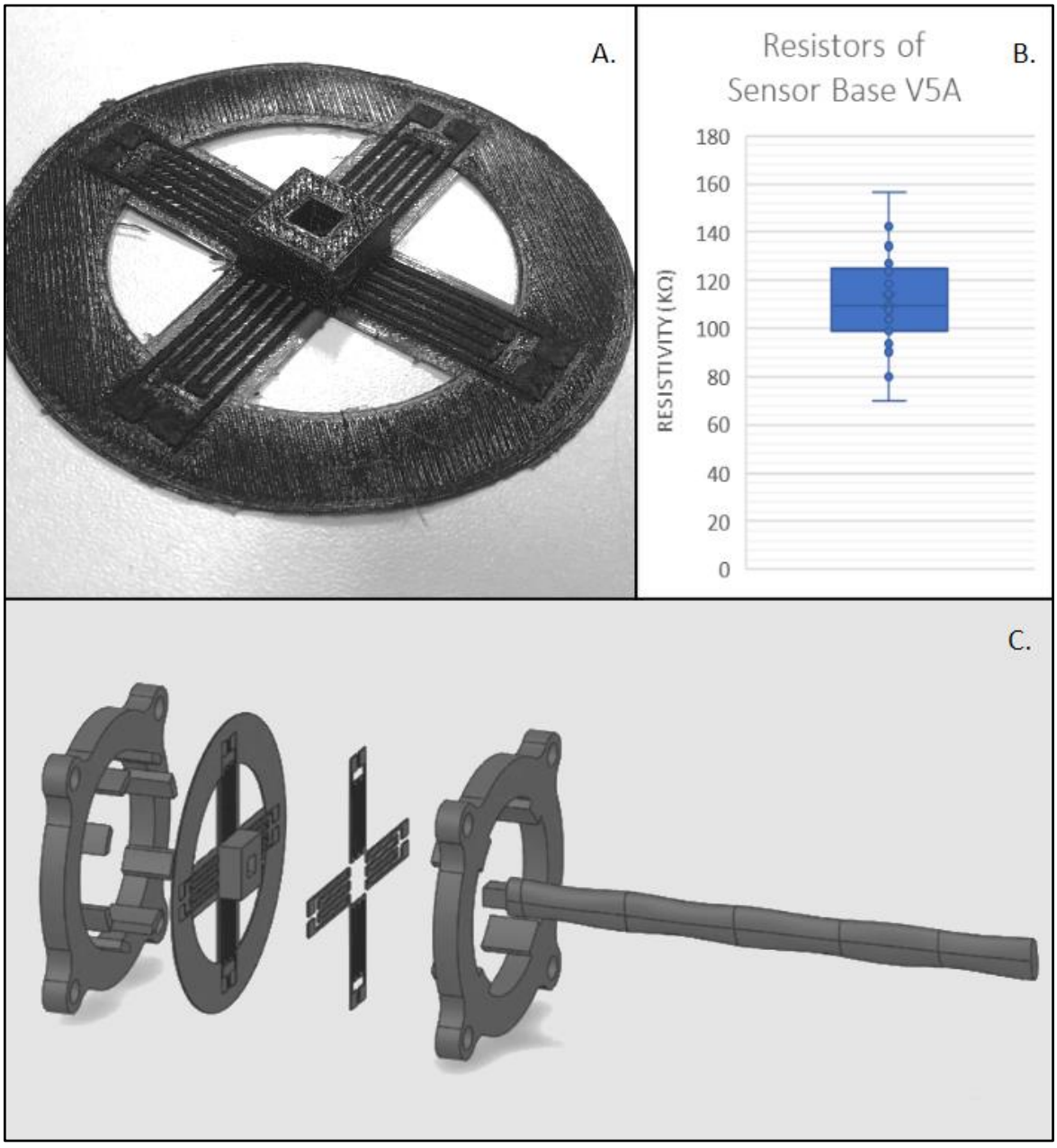

Figure 1. A: The membrane and sensors in final configuration. **B:** Boxplot showing the measured resistivity at rest for all 32 tested sensor gauges. **C:** Exploded view of the final model.

2.3 - Initial Testing

Once the design was considered definitive, a total of eight sensor bases were printed and each base was given a minimum of 12 hours to adjust to its environment. The primary objective is to verify the functionality of the sensor. To achieve this, a multimeter is used to record the resistivity of each strain gauge. This measurement assesses the repeatability of the design. Figure 1.B illustrates the boxplot representation of the measured resistivity values. An average resistivity of 111.6 ± 18.1 kΩ is found. While these findings demonstrate that all printed strain gauges do work, it became evident that the strain gauges are lacking reproducibility.

2.4 - Data Acquisition

In order to record the sensor output, each strain gauge is connected to a voltage divider circuit. For each direction of measurement, there are two active sensors. When one of the strain gauges is compressed due to the motion of the whisker, the opposite strain gauge is extended, therefore both contributing to the same voltage drop. Each pair of sensors are connected to an analog differential input on the DAQ (National Instruments, USB-6003). This setup filters out a large amount of background noise present in all sensors, thereby achieving a better signal-to-noise ratio.

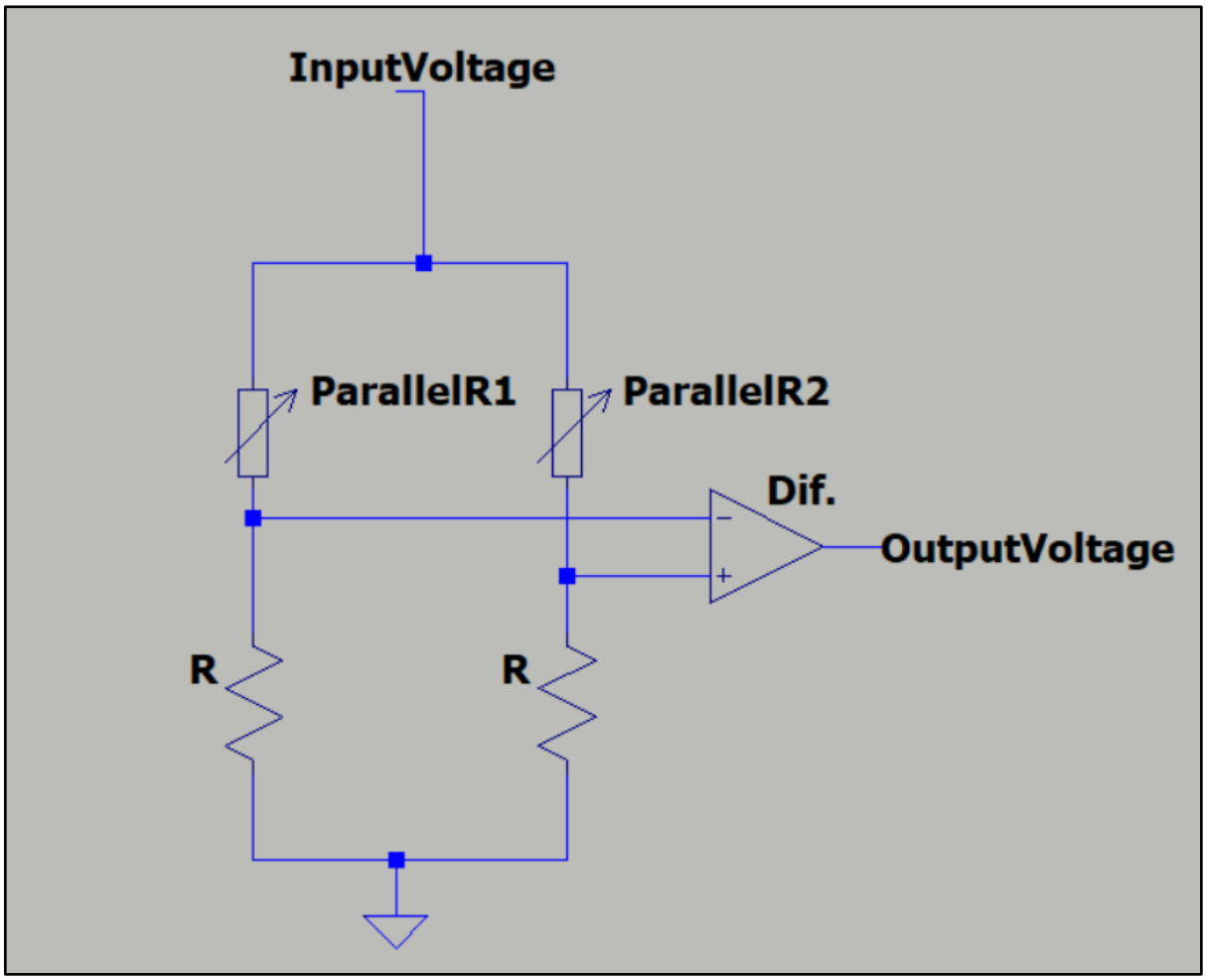

Figure 2: Schematic of the electronic circuit corresponding to the strain gauges parallel to the flow.

3. Experimental Section

3.1 - Experimental Setup

For the testing of the sensor, a water circulation flume is used (5L Loligo Systems Swim Tunnel), as illustrated in Figure 3.C. The flow is controlled by an electric motor that can achieve a maximal flow speed of 82 cm/s. In the experiment, six different flow settings were used, ranging from 2.4 to 30.8 cm/s. The Reynolds number corresponding to these settings ranged from ≈180 to ≈2500, indicating a laminar flow. Also another sensor output is recorded while leaving the motor turned off.

In the testing of the sensor, three different whiskers are used, of which two are based on the seal whisker. One seal whisker is attached at a 0 degrees orientation, with 0 degrees indicating that the minor axis is pointing towards the flow. The other seal whisker is attached at a 90 degree orientation, with 90 degrees indicating that the major axis is pointing towards the flow. Also a cylindrical whisker is attached, where the orientation was irrelevant because. All the whiskers are submerged by 5 cm while being subjected to the seven flow settings. To ensure that the measurement is accurate, the whisker is allowed to settle for 10 seconds after a change in flow. The sensor output is recorded for 10 seconds at a sampling rate of 1 kHz, spread over 10 samples. When a total of 70 samples is recorded, the whisker is swapped for another whisker. For each flow and whisker a total of 20 seconds is recorded, therefore the same whisker is used twice.

3.2 - Data Processing

For the processing of the gathered data, a Python code is made. This code consists of four individual parts, starting with the Preprocessing. This step centres all data around the mean of each sample, by subtracting the sample mean from every datapoint in that sample. This approach allows for a direct comparison of every measurement, without modifying the data. This new data frame is used by the remaining three steps, which are the plotting of Amplitude vs. Time, plotting of Amplitude vs. Flow and the Frequency analysis. The code and corresponding explanation is attached to this report in the Google Drive.

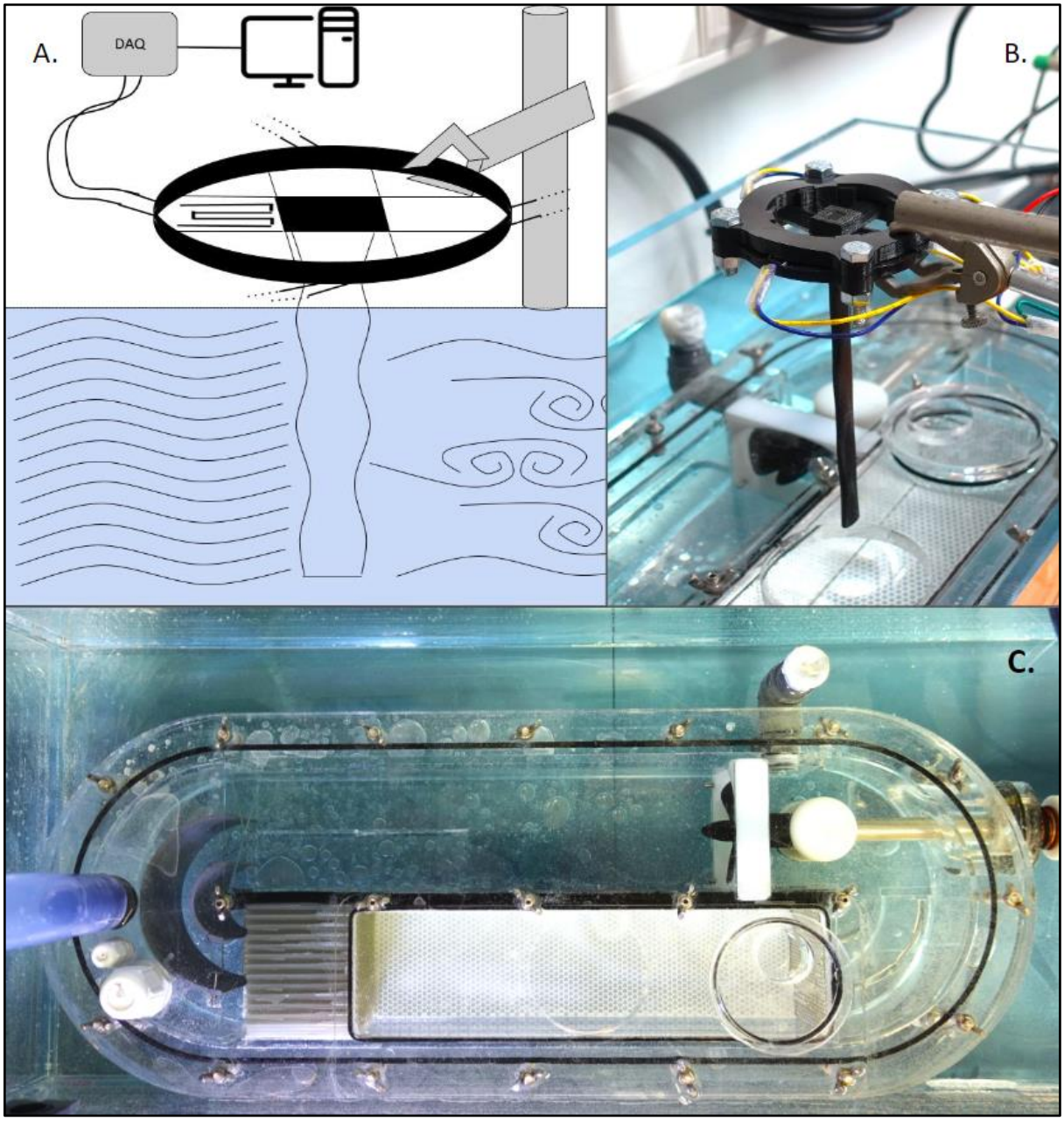

Figure 3. A: Schematic drawing of the experimental setup. **B:** Sensor in clamp, floating above the water circulation flume. **C:** Birdseye view of the water circulation flume. On the top right, the motor and connected propeller is located. In the centre, there is a circular hole through which the whisker can be inserted.

4. Results

4.1 - Temporal Analysis of Whisker Vibration

During the experimentation, when the different whiskers are subjected to flow speeds up to 8 cm/s, no clear vibrations are observed in either the direction parallel or perpendicular to the flow. When plotted against time, the sensor output matches this observation, in the sense that independent of the whisker type or orientation, the same stable output is achieved. The maximal sensor output, as displayed in Figure 4.B and C also confirm this observation. Notably, at these flow speeds up to 8 cm/s, the average maximal amplitude remains stable within a range of 4 to 6 mV for both sensor directions. It is worth noting that this non-zero output, as opposed to the output at 0 cm/s, can be explained by movement artefacts caused by the running motor.

Upon increasing the flow speed beyond 8 cm/s, the whiskers started to vibrate both parallel and perpendicular to the flow. With this, also a difference in vibration between the whiskers becomes noticeable. The 0 degree whisker remains stable, even up to a flow speed of 31 cm/s, while the cylinder and the 90 degree whisker start to vibrate violently. Again, this observation is supported by the sensor output when plotted against time, where the 0 degree whisker remains stable, whereas the other two whiskers are vibrating. Figure 4.A visually represents the sensor output corresponding to the VIVs, where a repetitive sinusoidal pattern can be observed, whereas the parallel output appears to show a more chaotic vibration. In Figure 4.C a slight drop of the average amplitude for the VIVs is observed with a flow speed increasing beyond 25 cm/s.

4.2 - Frequency Analysis of Whisker Vibration

The results presented in section 4.1 demonstrate a stable output when the whiskers are subjected to a flow of up to 8 cm/s. These findings can also be explained by the extrapolated frequencies of the sensor output. In Figure 5.A, the VIV frequencies are shown for the 90 degree whisker, showing stable, low-magnitude frequencies for flow speeds lower than 8 cm/s. However, when the flow speed is increased beyond 8 cm/s, the frequency shows a distinctive peak magnitude, indicating the presence of the VIVs.

For each of the whiskers, the expected frequency at which the VIV are occurring (fVIV) is calculated, by making use of the Strouhal number. Figure 5.B shows the comparison of the expected fVIV and the measured frequency for the 0 degree whisker, while Figure 5.C does this for the 90 degree whisker. These plots are closely connected to the results shown in section 4.1, in that the 90 degree whisker follows the expected frequencies with good agreement, indicating the presence of VIVs, whereas the 0 degree whisker is suppressing the VIVs.

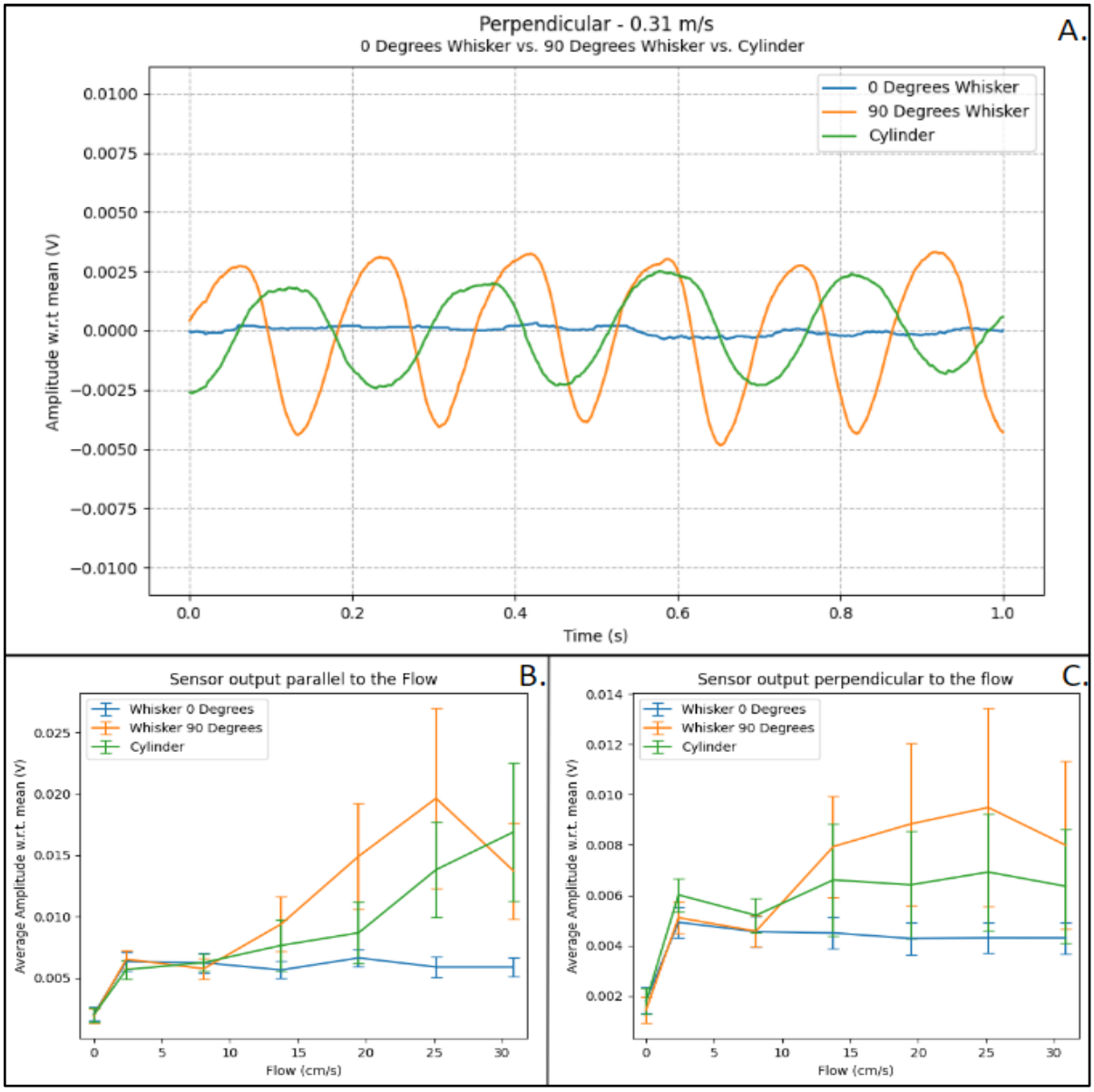

Figure 4. A: Graph of the sensor outputs for three different whiskers, measured in the perpendicular direction (VIV) at a flow rate of 31 cm/s. **B:** Graph displaying the averaged absolute maximal voltage output versus the flow speed, for the sensors parallel to the flow. **C:** Graph displaying the averaged absolute maximal voltage output versus the flow speed, for the sensors perpendicular to the flow. (VIV).

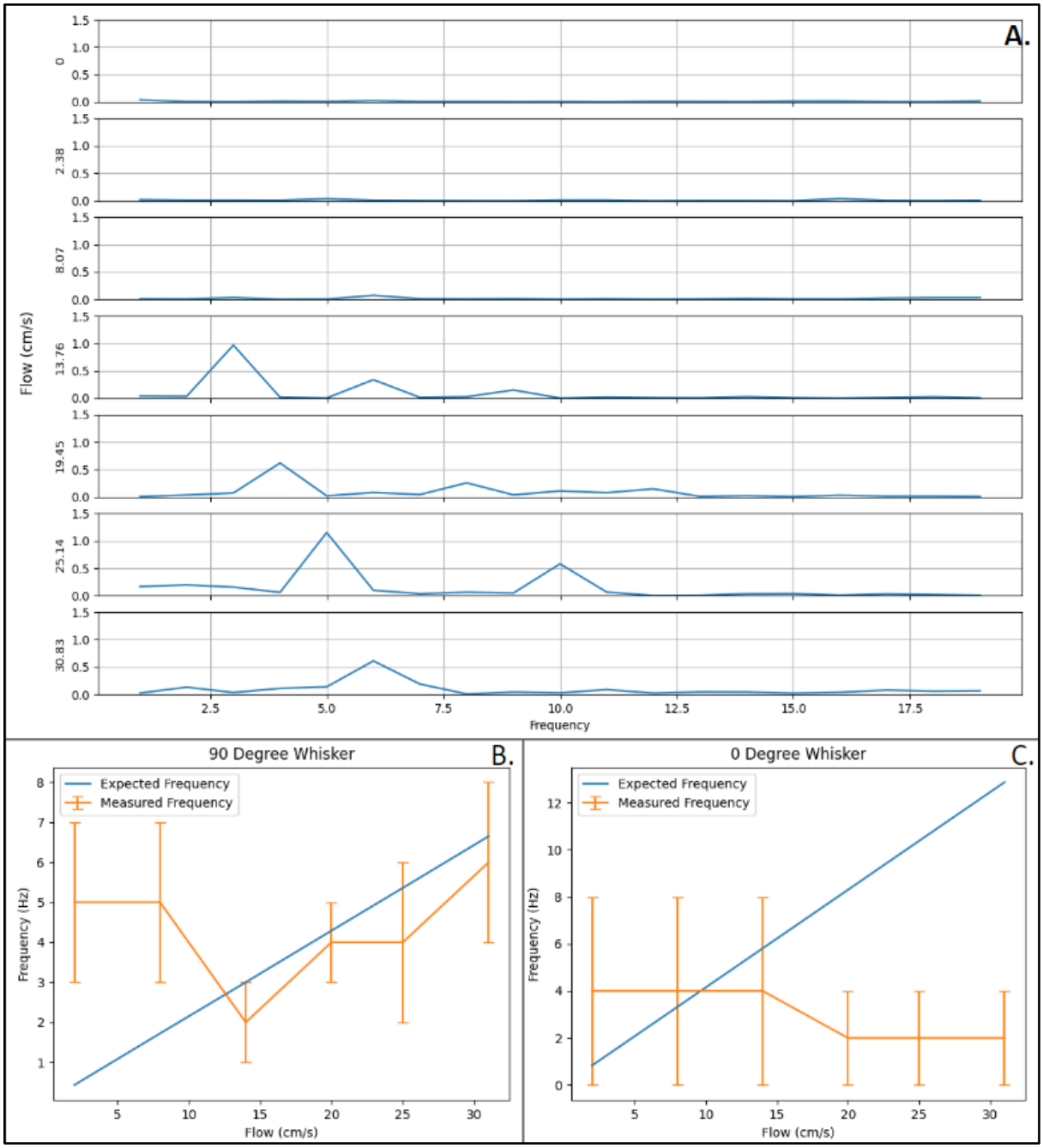

Figure 5. A: Graph plotting the amplitude versus frequency, for a range of 0 to 20 Hz, for every second measurement of the 90 degree whisker as measured by the sensors perpendicular to the flow. **B:** Graph of the expected and measured frequency at which the VIV are occurring for the whisker at a 0 degrees orientation. **C:** Graph of the expected and measured frequency at which the VIV are occurring for the whisker at a 90 degrees orientation.

5. Conclusion

The main objective of this report is to design and make a fully 3D printed sensor system. This study proves that it is possible to print a sensor, by making use of one FDM printer. The generated output matches the observations, and shows that the seal whisker morphology can indeed suppress VIVs. However, while the sensor did produce a consistent output, the repeatability of the printed strain gauges was less than optimal. Nonetheless, the technique that this study shows has great potential for future research.

6. Discussion

6.1 - Quality of Printing, Sensor Wiring and Experimental Design

However, besides the success in developing the sensor, it is important to mention the limitations caused by the quality of the printed sensor. As mentioned before, the resistivity of the printed strain gauges are not consistent. The printed strain gauges show a large variation in resistivity. This could potentially have influenced the accuracy of the sensor output.

Furthermore, the wiring that connects the sensor to the DAQ was not firmly fixed, but rather pushed through the connection pads on the strain gauges. This allows the wires to move freely, and therefore this results in a large change in resistivity whenever the wiring is touched only slightly. This implies that for every time the whisker is changed for a different version, the resistivity of the sensor would change and therefore the output would be different at each measurement. In further development of this sensor system, these issues need to be addressed.

Additionally, an issue needs to be addressed that is found during the processing of the experimental data. All the data is gathered in one-second samples, indicating that the maximal resolution that could be obtained in the frequency domain is limited to 1 Hz. This resolution proved to be too inaccurate to compare with the expected frequencies, which were all calculated with two significant digits. All these problems combined have impacted the precision and accuracy of the gathered data, which may have resulted in an inaccurate depiction of the performance of the produced sensor.

6.2 - Time Constraints

During this project, it is important to note that only a limited amount of time of eleven weeks was available to design and test the sensor. Before the design process started however, an issue with the printing of flexible materials had to be solved. Without a guideline to print with this machine, the design could not be completed. A summary of this problem and its solution can be found in Appendix A. The process of troubleshooting the printing process took five weeks, leaving only six more weeks to develop the sensor. Due to this limited time frame, the design of the sensor was completed hastily, resulting in compromises in achieving the desired quality of the sensor.

7. Future Work

As explained in the discussion section of this report, many problems can be addressed to improve the quality of the developed sensor. First of all, more attention should be focussed towards the optimization of the printer settings. By exploring and refining all the different settings that can be adjusted inside the printer system, the quality of each printed sensor can be improved. For this, also the location and orientation of the sensor on the print bed can be considered. Secondly, an improvement in printing resolution can be achieved by changing the nozzle diameter. While a 400-micrometre nozzle was used during this project, smaller nozzles are readily available. By implementing this smaller resolution, the design of the strain gauges can be improved. Thirdly, the design of the strain gauges, and corresponding sensor base and clamp can be improved by reducing its overall size. The strain gauges can be optimised, by making use of the increased resolution and reducing the overall length. This will result in a more sensitive response to a change in strain. The clamps can be improved by allowing for a better integration of the wiring that connects the sensor to the DAQ. Also a more robust attachment can be designed upon the sensor clamp to allow for a standardised experimental setup.

Besides the improvement of the sensor design, also multiple new experiments can be performed to further test the (redesigned) sensor. Firstly, a new setup should be created that can calibrate the sensor, so that the voltage output can be linked to the whisker angle. Secondly, the performance of the sensor should be tested for its intended function. Now only the working principle of the strain gauge has been tested. After this, also the change in vibration should be examined when the whiskers are subjected to a wake. With this, multiple different whiskers can be experimented with to find the different response between i.e. the grey seal whisker and the harbour seal whisker.

It is important to note that for every following experiment, a sample time of at least 10 seconds should be used, to make sure that the frequency resolution will be improved with respect to the achieved resolution in this report. A better streamlined and more adaptable code may also help for the processing of the data.

Bibliography

[1] *Vortex induced vibrations | Fluid Mechanics Research Laboratory*. (n.d.). https://uwaterloo.ca/fluid-mechanics-research-lab/research/vortex-induced-vibrations

[2] Hanke, W., Witte, M. D., Miersch, L., Brede, M., Oeffner, J., Michael, M., Hanke, F. D., Leder, A., & Dehnhardt, G. (2010). Harbor seal vibrissa morphology suppresses vortex-induced vibrations. *The Journal of Experimental Biology*, *213*(15), 2665–2672. https://doi.org/10.1242/jeb.043216

[3] Zheng, X., Kamat, A. M., Harish, V. S., Cao, M., & Warkiani, M. E. (2021). *Optimizing Harbor Seal Whisker Morphology for Developing 3D-Printed Flow Sensor*. https://doi.org/10.1109/transducers50396.2021.9495504

[4] Zheng, X., Kamat, A. M., Krushynska, A., Cao, M., & Warkiani, M. E. (2022a). 3D Printed Graphene Piezoresistive Microelectromechanical System Sensors to Explain the Ultrasensitive Wake Tracking of Wavy Seal Whiskers. *Advanced Functional Materials*, *32*(47), 2207274. https://doi.org/10.1002/adfm.202207274

[5] Zheng, X., Kamat, A. M., Cao, M., & Warkiani, M. E. (2022b). Wavy Whiskers in Wakes: Explaining the Trail-Tracking Capabilities of Whisker Arrays on Seal Muzzles. *Advanced Science*, *10*(2), 2203062. https://doi.org/10.1002/advs.202203062

[6] Correia, V., Caparros, C., Casellas, C., Francesch, L., Rocha, J., & Lanceros-Méndez, S. (2013). Development of inkjet printed strain sensors. *Smart Materials and Structures*, *22*(10), 105028. https://doi.org/10.1088/0964-1726/22/10/105028

[7] *All-Inkjet Printed Strain Sensors*. (2013, December 1). IEEE Journals & Magazine | IEEE Xplore. https://ieeexplore.ieee.org/abstract/document/6574213

[8] Agarwala, S., Goh, G. L., Yap, Y. C., Yu, H., Yeong, W. Y., & Tran, T. (2017). Development of bendable strain sensor with embedded microchannels using 3D printing. *Sensors and Actuators A-physical*, *263*, 593–599. https://doi.org/10.1016/j.sna.2017.07.025

[9] Yan, H., Liu, S., Wen, N., Yin, J., & Jiang, H. (2023). Self-Healing Flexible Strain Sensor Fabricated Through 3d Printing Template Sacrifice for Motion Monitoring with Enhanced Healing and Mechanical Performance. https://doi.org/10.2139/ssrn.4448766

[10] Georgopoulou, A., Srisawadi, S., Wiroonpochit, P., & Clemens, F. (2023). Soft Wearable Piezoresistive Sensors Based on Natural Rubber Fabricated with a Customized Vat-Based Additive Manufacturing Process. *Polymers*, *15*(10), 2410. https://doi.org/10.3390/polym15102410

[11] Maurizi, M., Slavič, J., Cianetti, F., Jerman, M., Valentinčič, J., Lebar, A., & Boltežar, M. (2019). Dynamic Measurements Using FDM 3D-Printed Embedded Strain Sensors. *Sensors*, *19*(12), 2661. https://doi.org/10.3390/s19122661

[12] *Eel 3D Printer Filament (90A) - NinjaTek*. (2021, April 12). NinjaTek. https://ninjatek.com/shop/eel/#print-guidelines

References used for the solving of the printing issues and improvement of the printing quality:

[13] N2d. (2020, July 11). *Tips for printing with Ninjatek EEL filament? [Online forum post]*. UltiMaker Community of 3D Printing Experts. https://community.ultimaker.com/topic/33220-tips-for-printing-with-ninjatek-eel-filament/#comment-268006

[14] *3D Printing Troubleshooting Guide - NinjaTek*. (2021, April 7). NinjaTek. https://ninjatek.com/support/troubleshooting-guide/

[15] NikThemechanic. (2018, December 5). *Difference between AA 0.4 and BB 0.4 nozzle [Online forum post]*. UltiMaker Community of 3D Printing Experts. https://community.ultimaker.com/topic/21217-difference-between-aa-04-and-bb-04-nozzle/

[16] *Support Community*. (n.d.). *How to fix under-extrusion.* https://support.makerbot.com/s/article/1667337580210

[17] *Support Community*. (n.d.). *How to fix feeder issues.* https://support.makerbot.com/s/article/1667337580379

[18] *Support Community*. (n.d.). *Material is ground down by the feeder.* https://support.makerbot.com/s/article/1667411553831

[19] *Support Community*. (n.d.). *Material settings.* https://support.makerbot.com/s/article/1667411286833

[20] Dsourced. (2023). Clogged 3D Printer Nozzle? – How to Prevent, Clean & Fix - 3DSourced. *3DSourced*. https://www.3dsourced.com/rigid-ink/clogged-extruder-nozzle-how-to-avoid-and-fix/

[21] *AMG3D - Aftermarket 3D printing products*. (2021, July 27). AMG3D. https://amg3d.com/

[22] SigvardsK. (2016, November 16). *TPU 95A filament under extursion? [Online forum post]*. UltiMaker Community of 3D Printing Experts. https://community.ultimaker.com/topic/15917-tpu-95a-filament-under-extursion/

Appendices

A. - Printing with Flexible Filaments

The Ultimaker S5 makes use of a Bowden drive extrusion. This means that the motor that drives the filament through the nozzle is not mounted directly at the extruder. The filament first travels through a connecting Bowden tube. In the case of the Ultimaker S5, the length of the Bowden tube is around 50 cm. For hard and stiff filaments, this is not a problem. However, when filaments get more flexible and more elastic, the motor will cause the filament to push on the Bowden tube, creating more friction and a less than optimal feeding angle. This will result in slipping and grinding down of the filament at the feeder motor and the clogging up of the nozzle at the extruder. The NinjaTek Eel is too flexible for this type of printer, and therefore this filament is not compatible with the Ultimaker S5.

To solve this problem, the best option is to use a direct drive feeder motor, instead of the Bowden drive. In this type of extrusion, the feeder motor would be attached directly to the extruder, resulting in a direct application of the force. There are direct drive FDM printers available on the market. As for the Ultimaker S5, there are compatible direct drive motors for sale for a price of €750,-[21], but these are not made by Ultimaker itself, so that might cause the warranty to expire. However, if the print only requires 40 cm of flexible filament or less, there is a cheaper solution to make a Bowden drive printer compatible. This requires a roll of stiff filament, like PLA or PVA, 40 cm of the flexible filament and super glue. Glue one end of the flexible filament to the end of the stiff filament, and let it set. Once dried up, the filament can be safely inserted into the feeder motor. The feeder motor will have more grip on the stiffer filament, and therefore can push the flexible material into the extruder. To make sure that no errors occur, it is important to turn off the flow sensor inside the Ultimaker S5 printer, because otherwise the print would abort before completion.

When printing with NinjaTek EEL, a printing temperature of 223^{o}C, a print speed of 20 mm/s and a flow rate of 96% yielded good results. The latter is to compensate for the thickness of the filament. In all prints, the Z-Hop setting should be disabled, for this ruins the print. The filament does not adhere properly to other materials. When designing a double extrusion print, make sure that the EEL body is well integrated into the other body; this means that the two bodies should overlap in one layer, so that the pattern of the second body is visible on the first body. An example of this is shown in Figure A1. Using this information, a consistent print of 100 µm thick can be achieved.

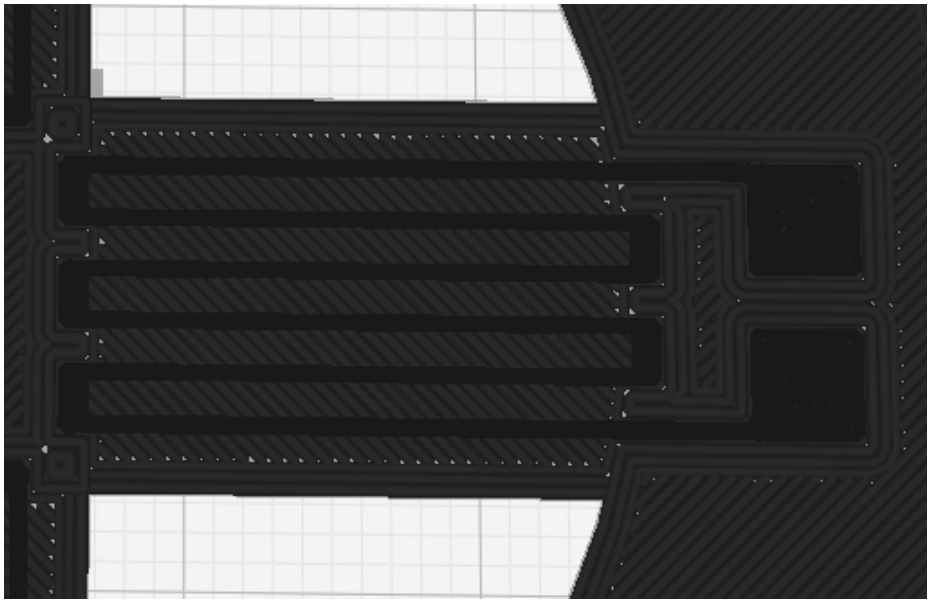

Figure A1: Example of integration of two separate bodies in the slicer

B. - Technical Drawings

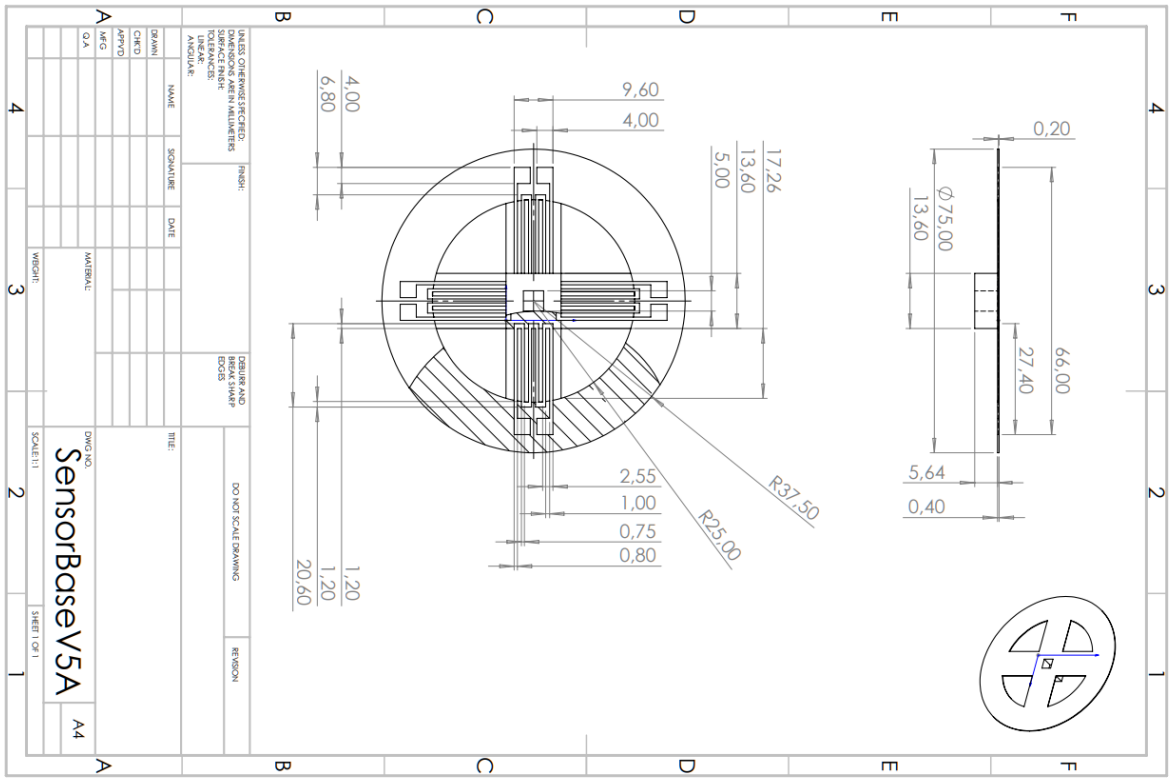

Figure A2: Technical drawing of the fifth (and final) version of the Sensor Base, size A.

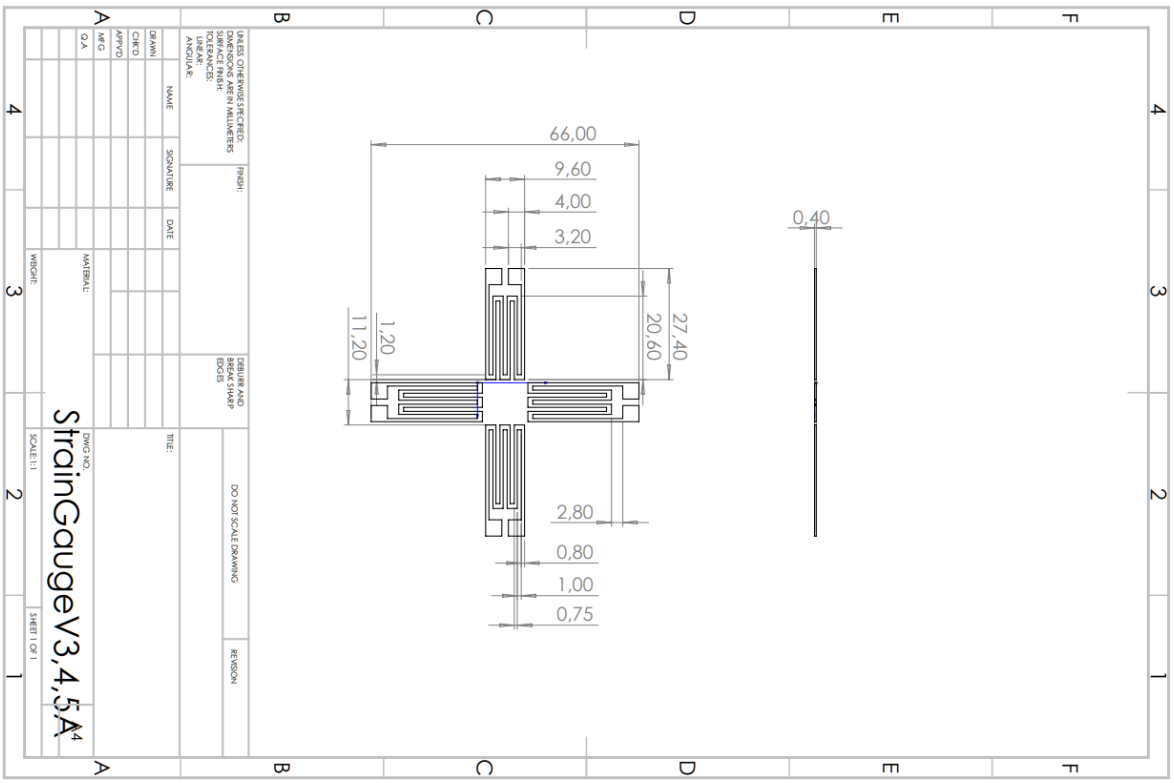

Figure A3: Technical drawing of the third (and final) version of the Strain Gauges, size A.

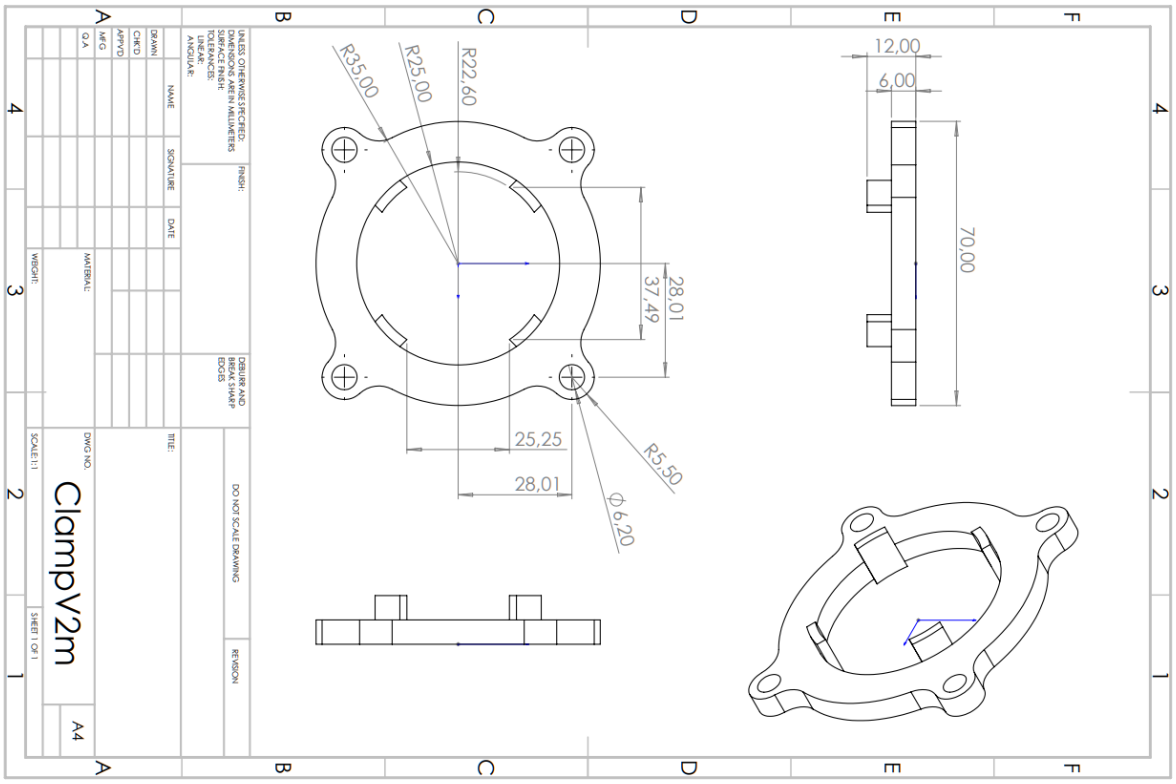

Figure A4: Technical drawing of the second (and final) version of the Clamp, male part of the set.

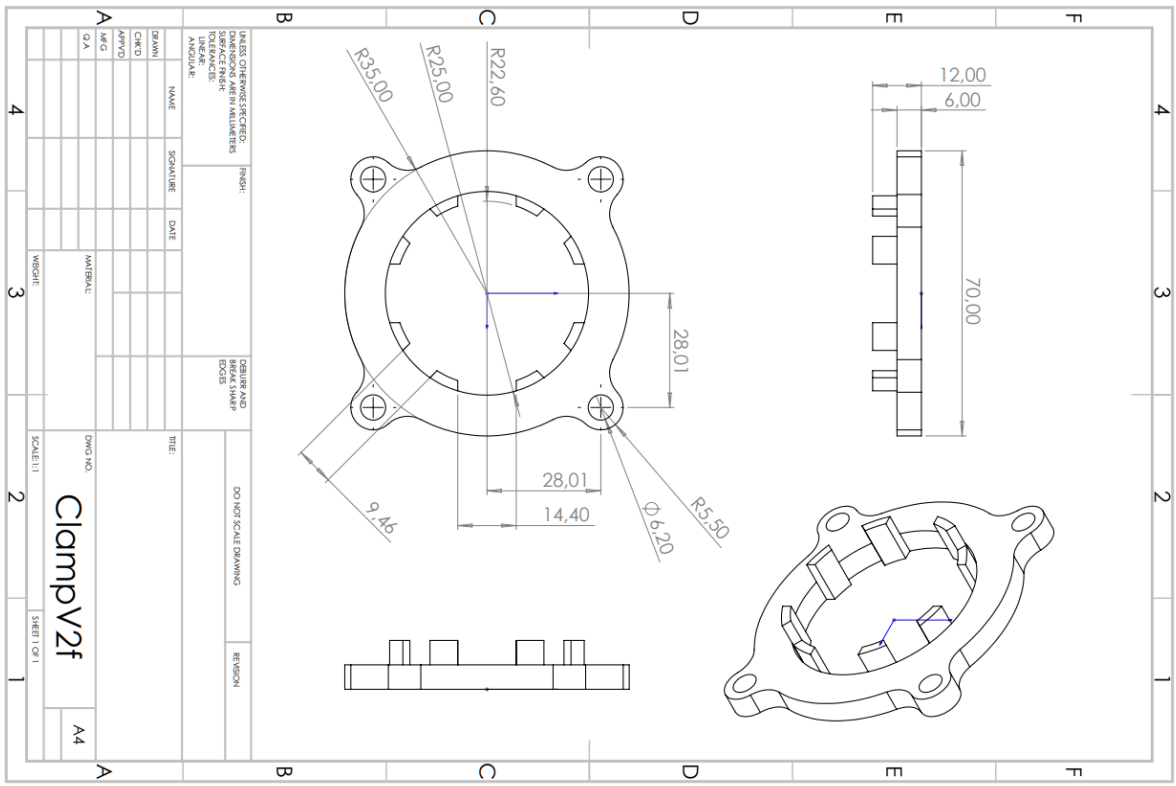

Figure A5: Technical drawing of the second (and final) version of the Clamp, female part of the set.

C. - Raw Data

Table A1: Resistivity for each of the printed sensor bases.

Resistor	Resistivity of Strain Gauge (kΩ), sorted per printed model							
	1	2	3	4	5	6	7	8
R1	93.9	94.7	108.0	115.6	156.5	134.2	103.9	100.0
R2	93.9	108.3	127.2	105.2	114.5	130.4	123.6	125.3
R3	100.5	107.7	117.8	90.3	125.6	115.2	98.8	92.5
R4	109.2	110.4	69.7	80.0	137.1	142.5	121.4	118.5
Average*	99.4 ± 7.3	105.3 ± 7.1	105.7 ± 25.2	97.8 ± 15.8	133.4 ± 17.9	130.6 ± 11.4	111.9 ± 12.4	109.1 ± 15.4

*The average resistance of all strain gauges combined was found to be 111.6 ± 18.1 kΩ.

Table A2: Characteristic Cross-Sectional Diameters of both the Grey Seal Whisker (V) and the Cylinder.

		Characteristic Cross-sectional Diameter (mm)
Grey Seal Whisker (V)	Minor Axis	5.06 ± 0.47*
	Major Axis	9.79 ± 0.10*
Cylinder		10.0 ± 0.40**

*The diameter was found by averaging 7 slices of the seal whisker model using the measurement tool in SolidWorks.

**The diameter was found by averaging 7 measurements of the printed cylinder, done with a digital calliper.

Table A3: Predicted and Measured Frequency of VIV and Standard Deviations

Whisker Type and Orientation	Free Stream Velocity (m/s)	Frequency of VIV (Hz)	
		fVIV - Calculated*	fVIV - Measured
Grey Seal Whisker (V) - 0°	0.02	0.83 ± 0.07	4 ± 4
	0.08	3.32 ± 0.28	4 ± 4
	0.14	5.81 ± 0.49	4 ± 4
	0.19	7.89 ± 0.67	2 ± 2
	0.25	10.38 ± 0.88	2 ± 2
	0.31	12.87 ± 1.09	2 ± 2
Grey Seal Whisker (V) - 90°	0.02	0.43 ± 0.00	5 ± 2
	0.08	1.72 ± 0.02	5 ± 2
	0.14	3.00 ± 0.03	2 ± 1
	0.19	4.08 ± 0.04	4 ± 1
	0.25	5.37 ± 0.05	5 ± 2
	0.31	6.65 ± 0.07	6 ± 2
Cylinder	0.02	0.42 ± 0.00	3 ± 4
	0.08	1.68 ± 0.01	2 ± 2
	0.14	2.94 ± 0.01	1 ± 0
	0.19	3.99 ± 0.02	2 ± 1
	0.25	5.25 ± 0.02	3 ± 1
	0.31	6.51 ± 0.03	4 ± 1

*Here $\frac{St \times U\infty}{D}$ is used as estimation for the predicted fVIV, where St is the Strouhal number, which is assumed to be 0.21 $U\infty$ is the free stream velocity and D is the characteristic cross-sectional diameter of the whisker / cylinder perpendicular to the flow. The values for D are retrieved from Table A2.

D. - Graphs

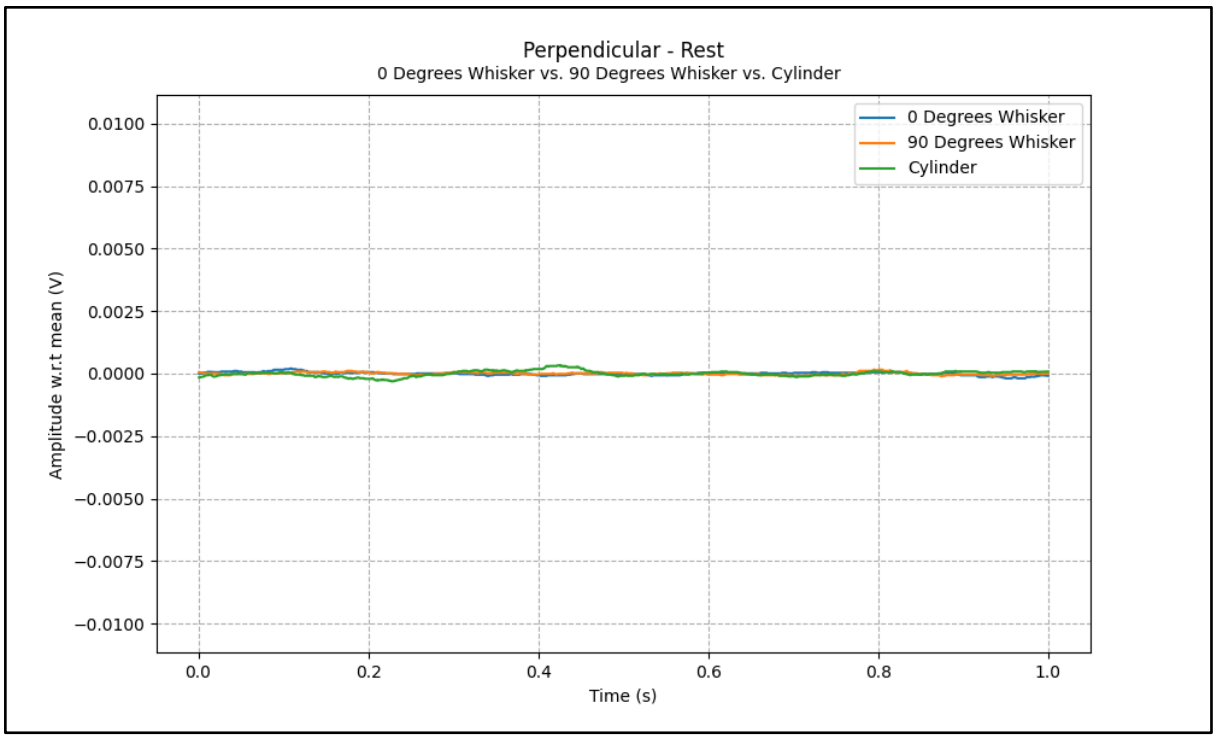

Figure A6: Graph of the (processed) sensor output versus time, as recorded by the sensor perpendicular to the flow, for a flow speed of 0 cm/s.

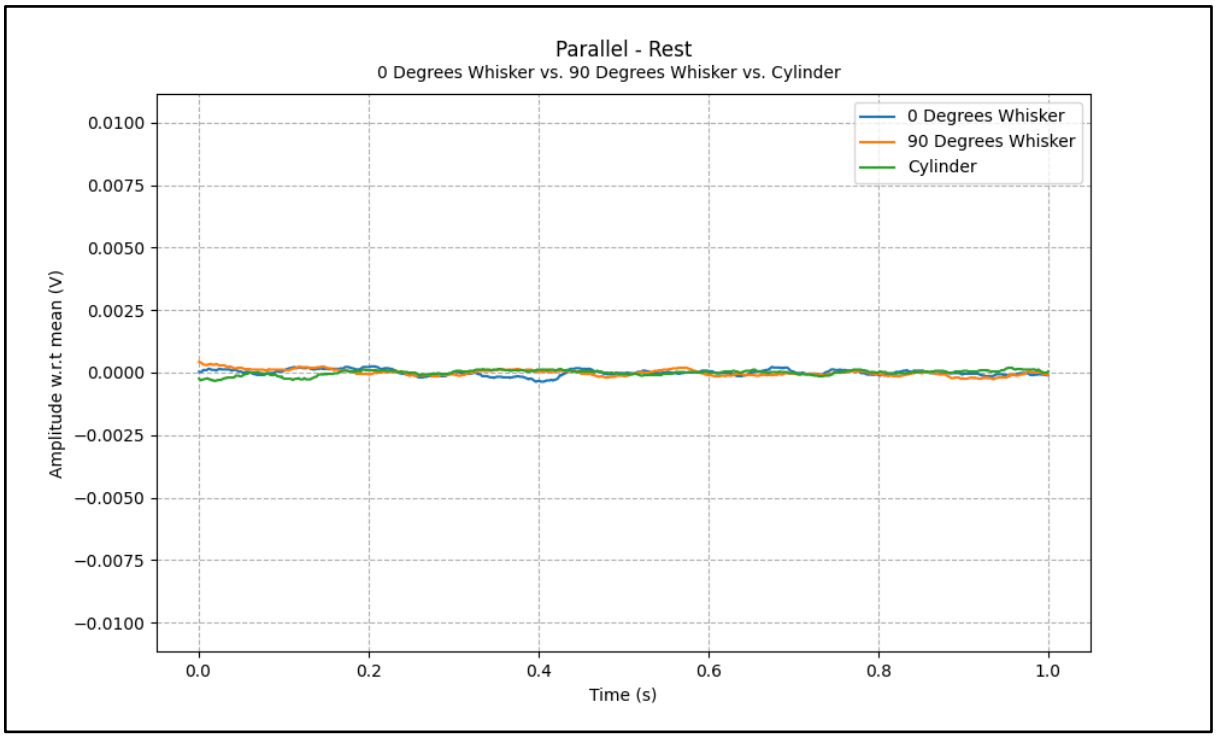

Figure A7: Graph of the (processed) sensor output versus time, as recorded by the sensor parallel to the flow, for a flow speed of 0 cm/s.

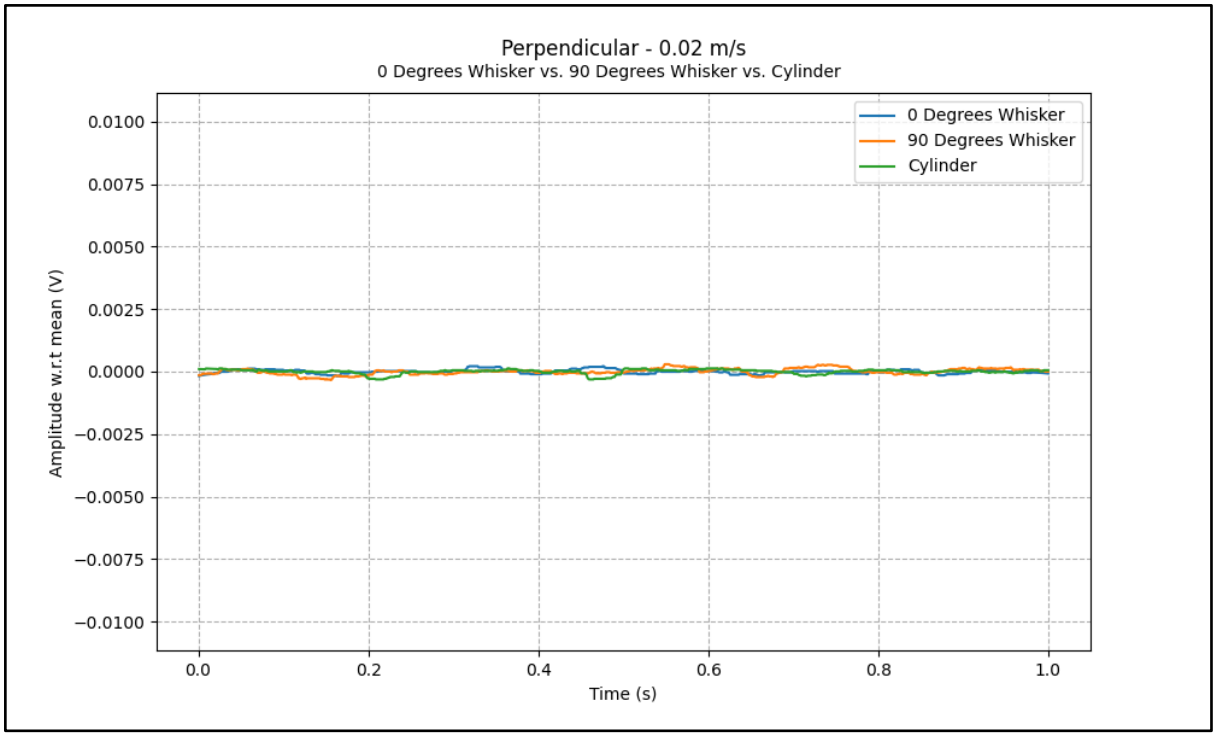

Figure A8: Graph of the (processed) sensor output versus time, as recorded by the sensor perpendicular to the flow, for a flow speed of 2 cm/s.

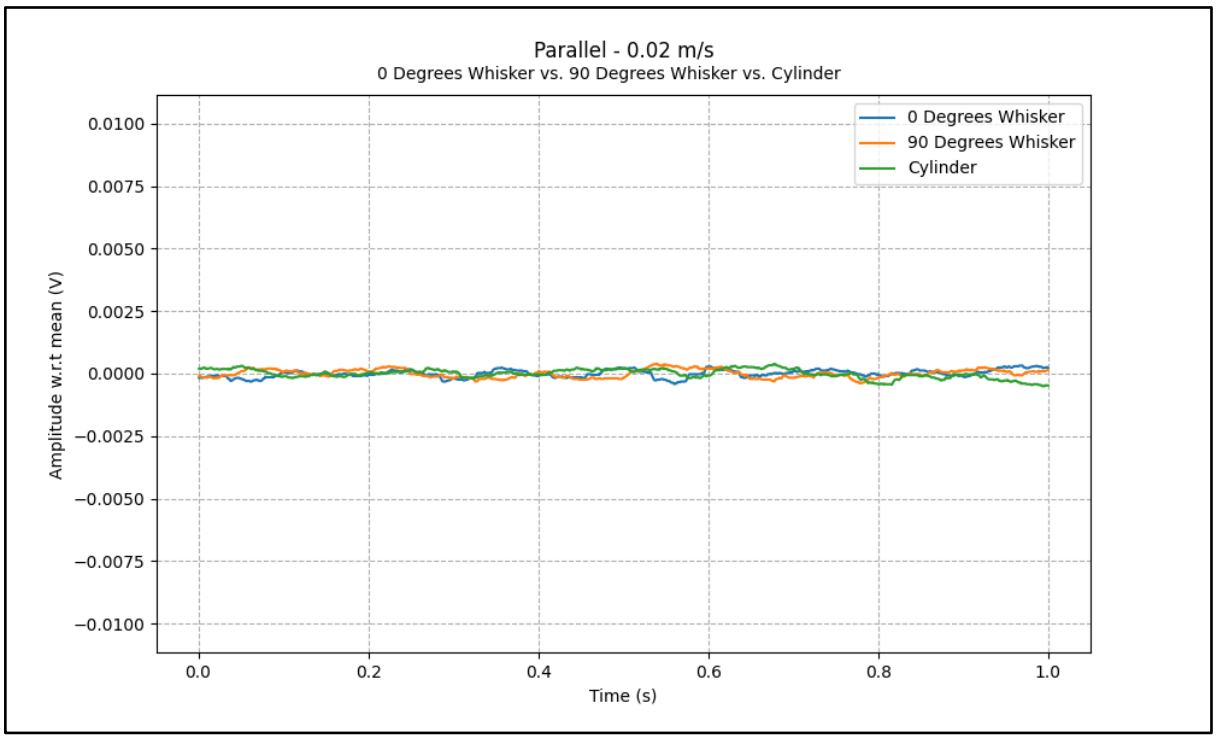

Figure A9: Graph of the (processed) sensor output versus time, as recorded by the sensor perpendicular to the flow, for a flow speed of 2 cm/s.

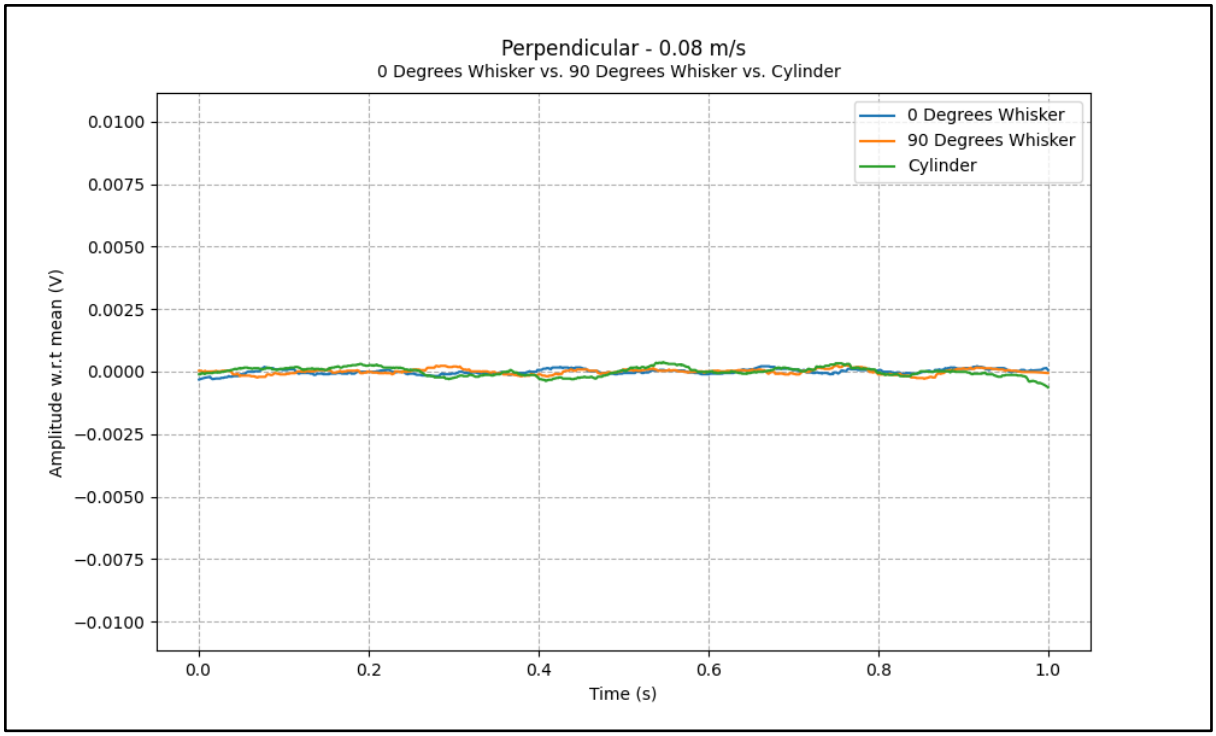

Figure A10: Graph of the (processed) sensor output versus time, as recorded by the sensor perpendicular to the flow, for a flow speed of 8 cm/s.

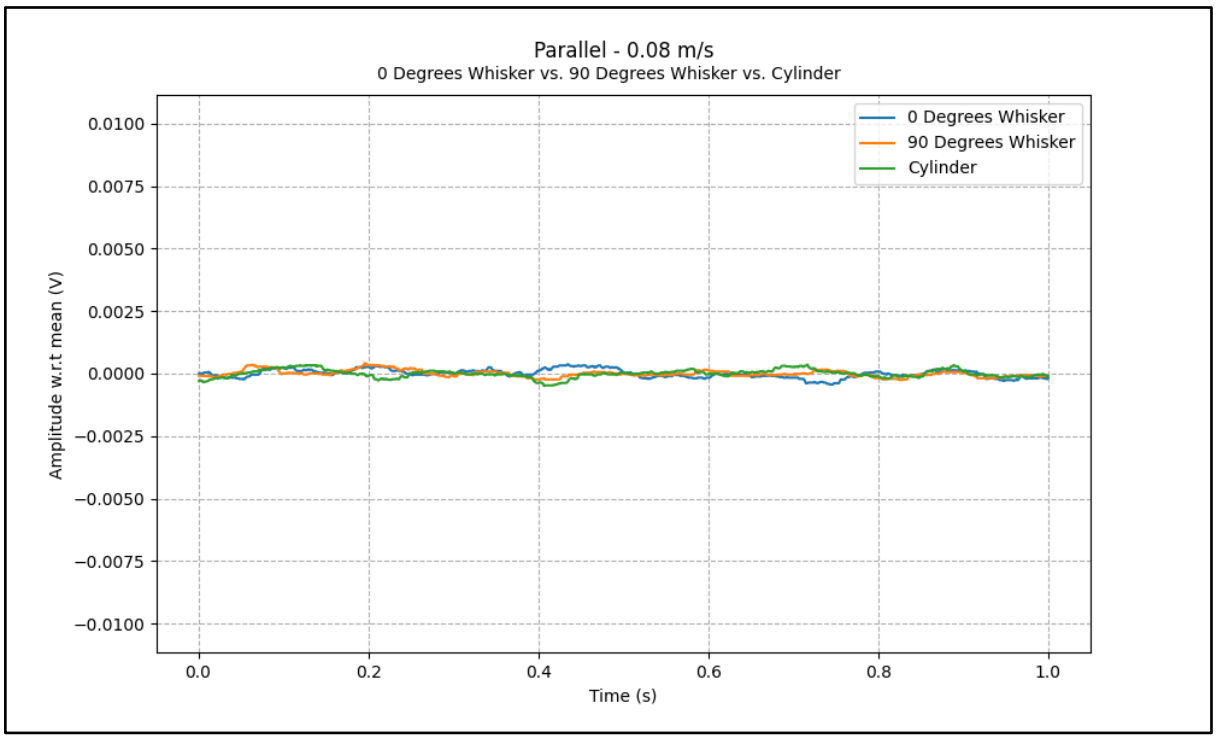

Figure A11: Graph of the (processed) sensor output versus time, as recorded by the sensor perpendicular to the flow, for a flow speed of 8 cm/s.

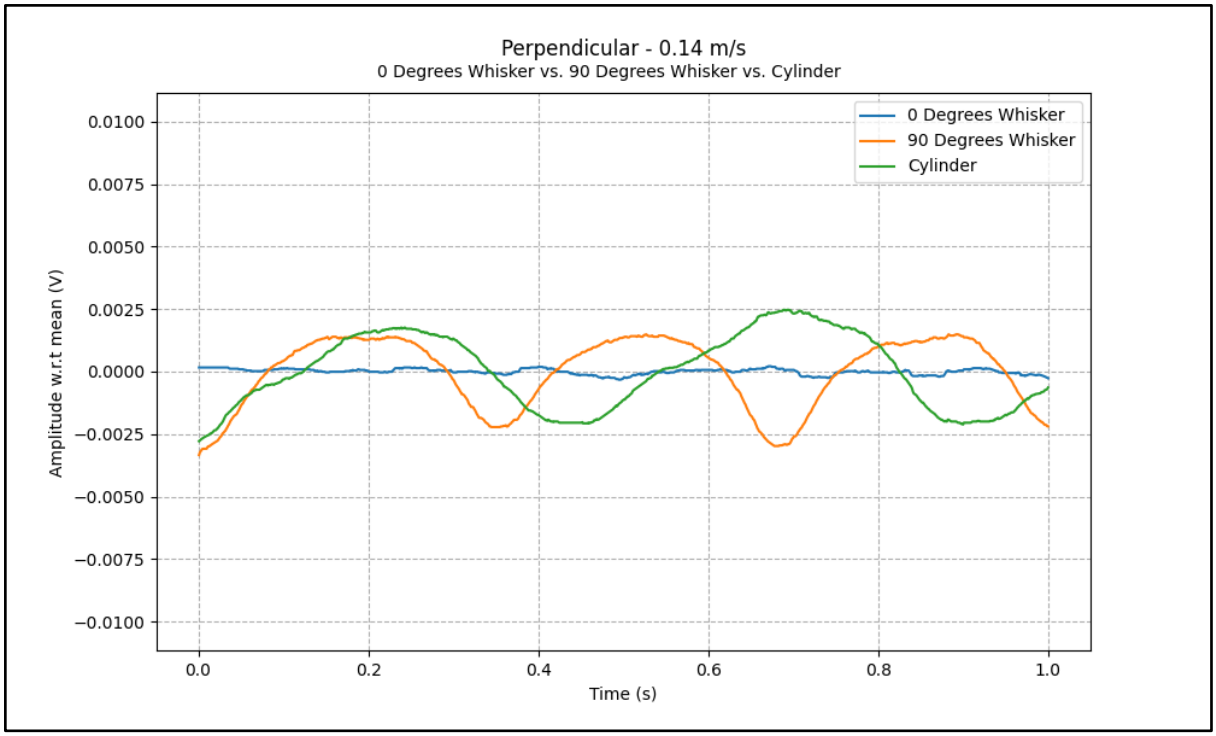

Figure A12: Graph of the (processed) sensor output versus time, as recorded by the sensor perpendicular to the flow, for a flow speed of 14 cm/s.

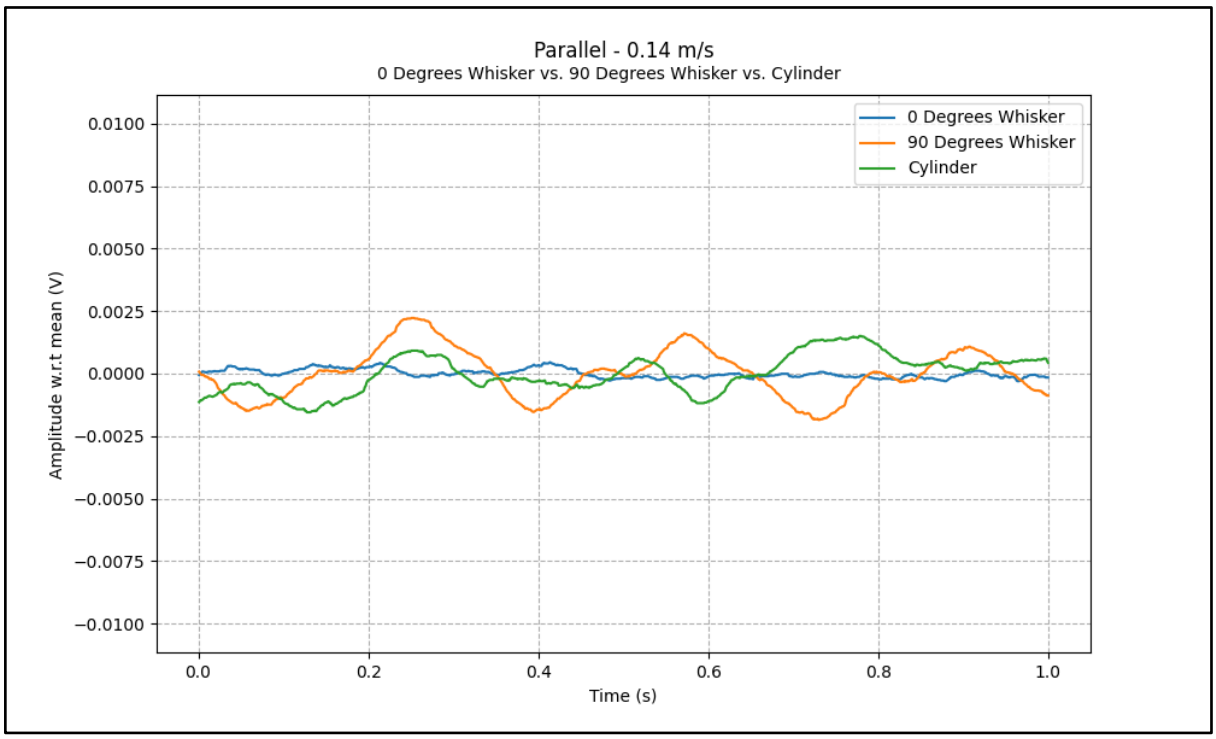

Figure A13: Graph of the (processed) sensor output versus time, as recorded by the sensor perpendicular to the flow, for a flow speed of 14 cm/s.

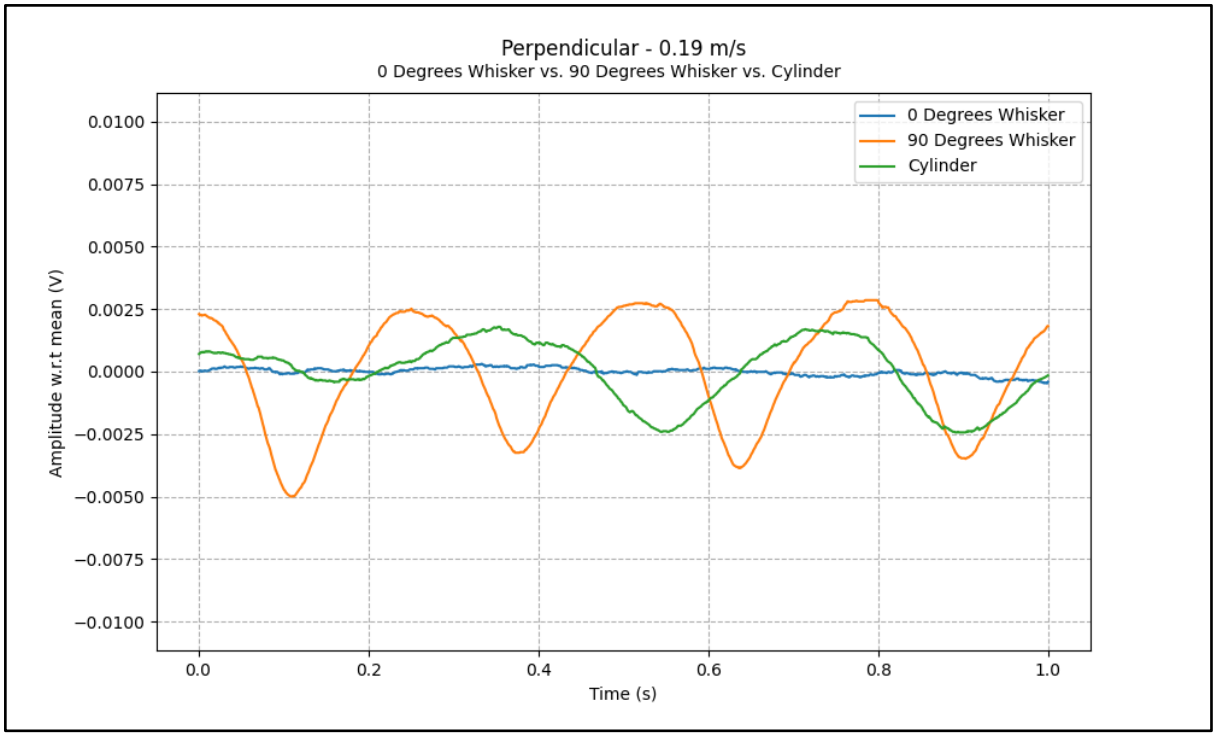

Figure A14: Graph of the (processed) sensor output versus time, as recorded by the sensor perpendicular to the flow, for a flow speed of 19 cm/s.

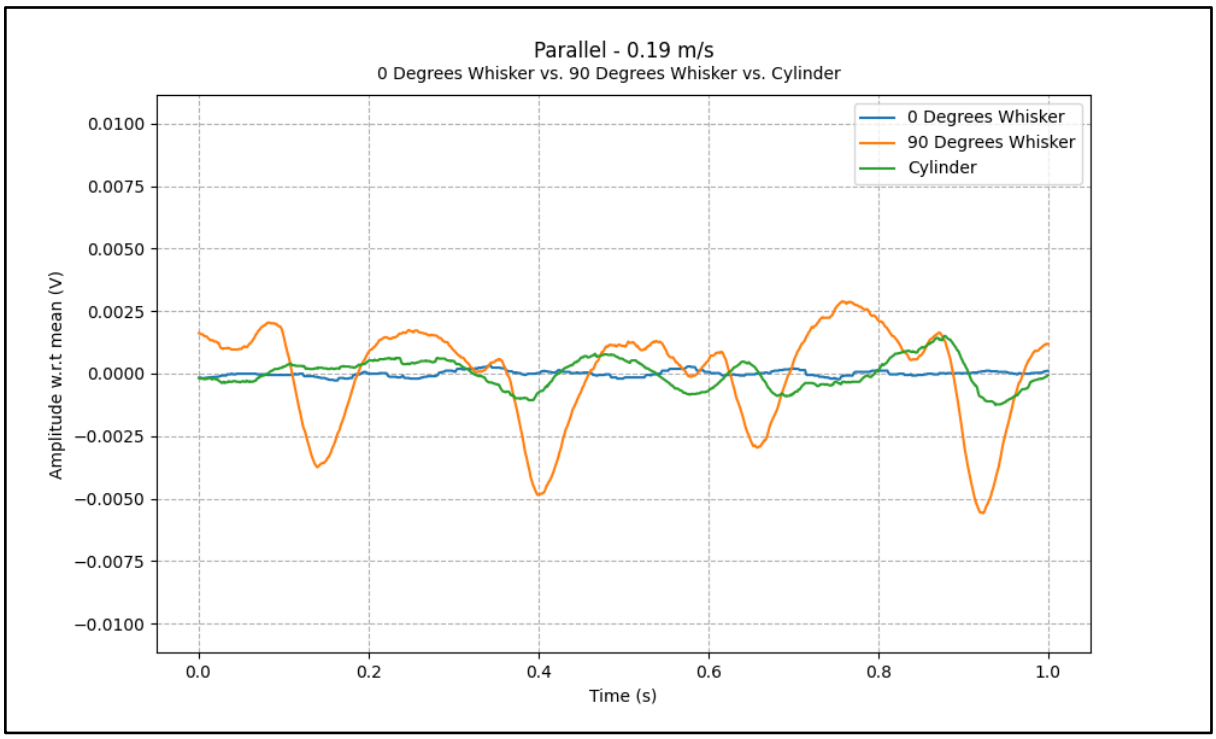

Figure A15: Graph of the (processed) sensor output versus time, as recorded by the sensor perpendicular to the flow, for a flow speed of 19 cm/s.

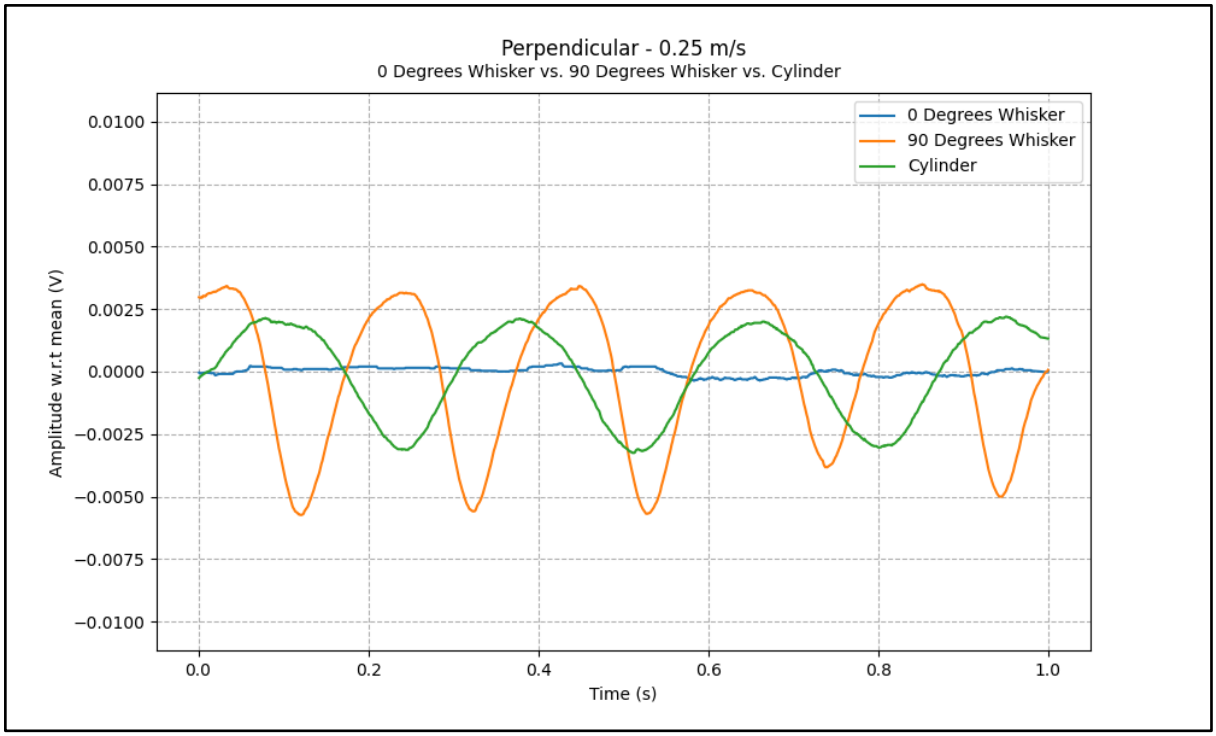

Figure A16: Graph of the (processed) sensor output versus time, as recorded by the sensor perpendicular to the flow, for a flow speed of 25 cm/s.

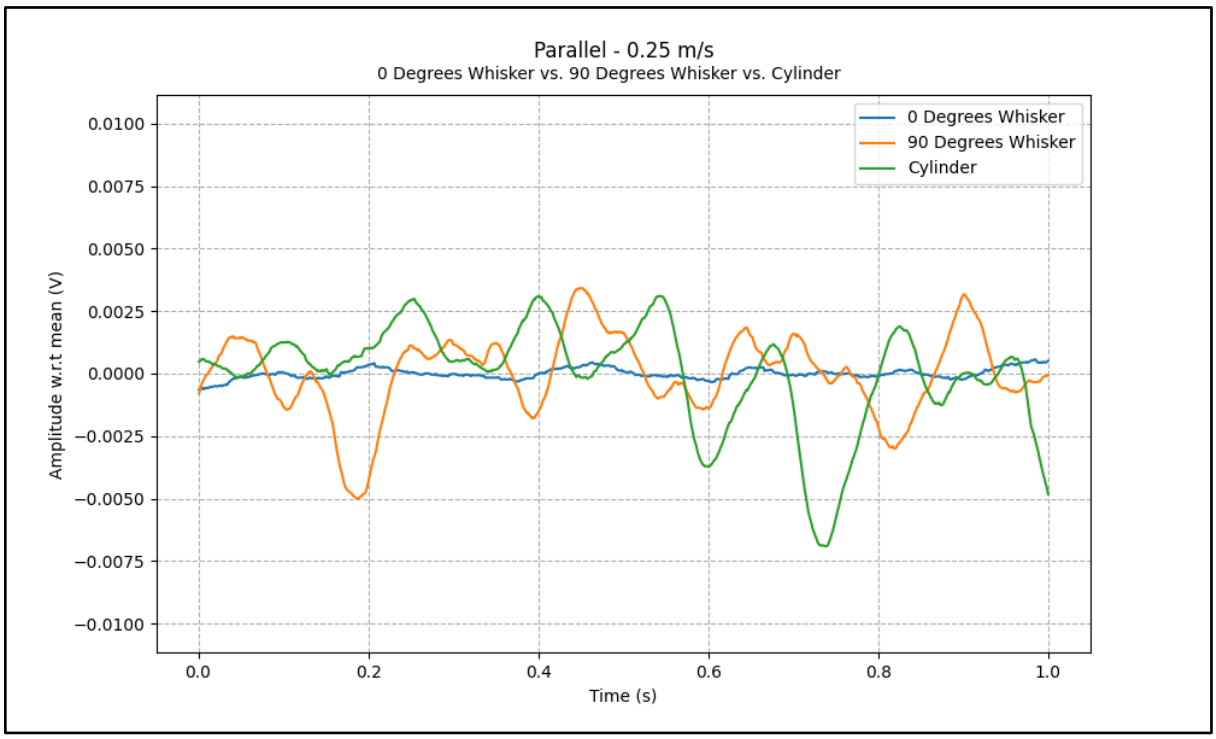

Figure A17: Graph of the (processed) sensor output versus time, as recorded by the sensor perpendicular to the flow, for a flow speed of 25 cm/s.

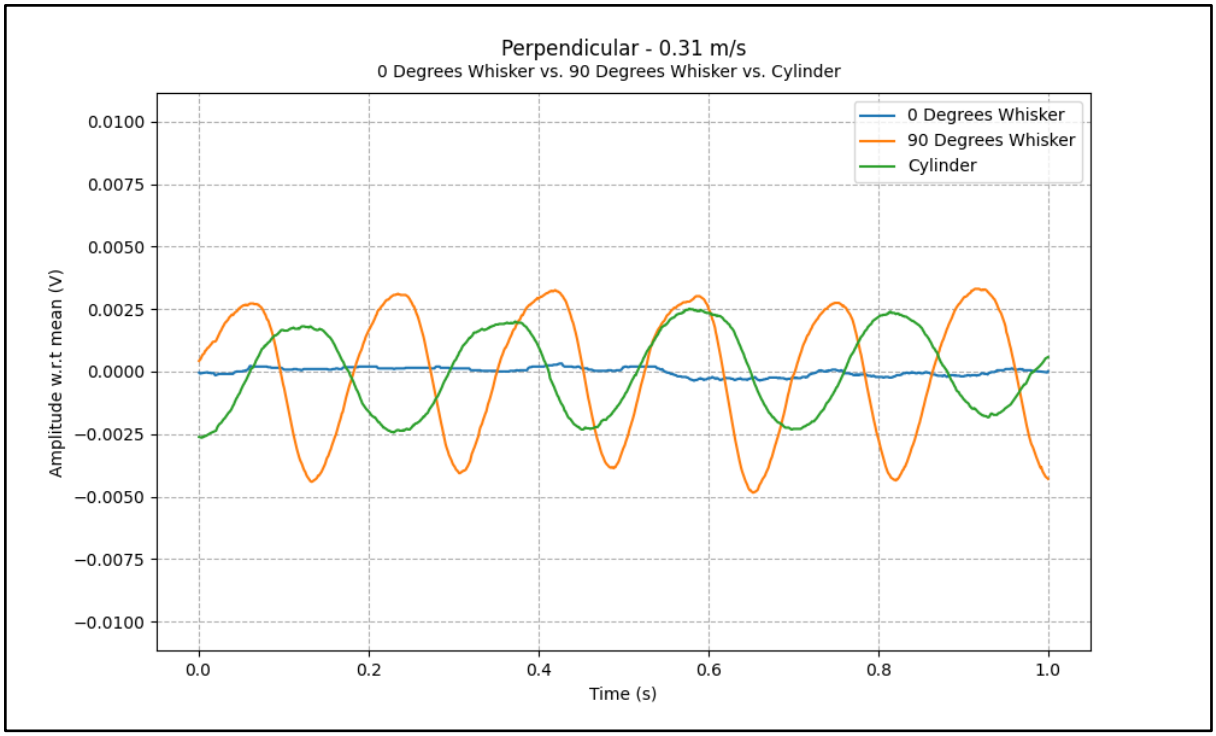

Figure A18: Graph of the (processed) sensor output versus time, as recorded by the sensor perpendicular to the flow, for a flow speed of 31 cm/s.

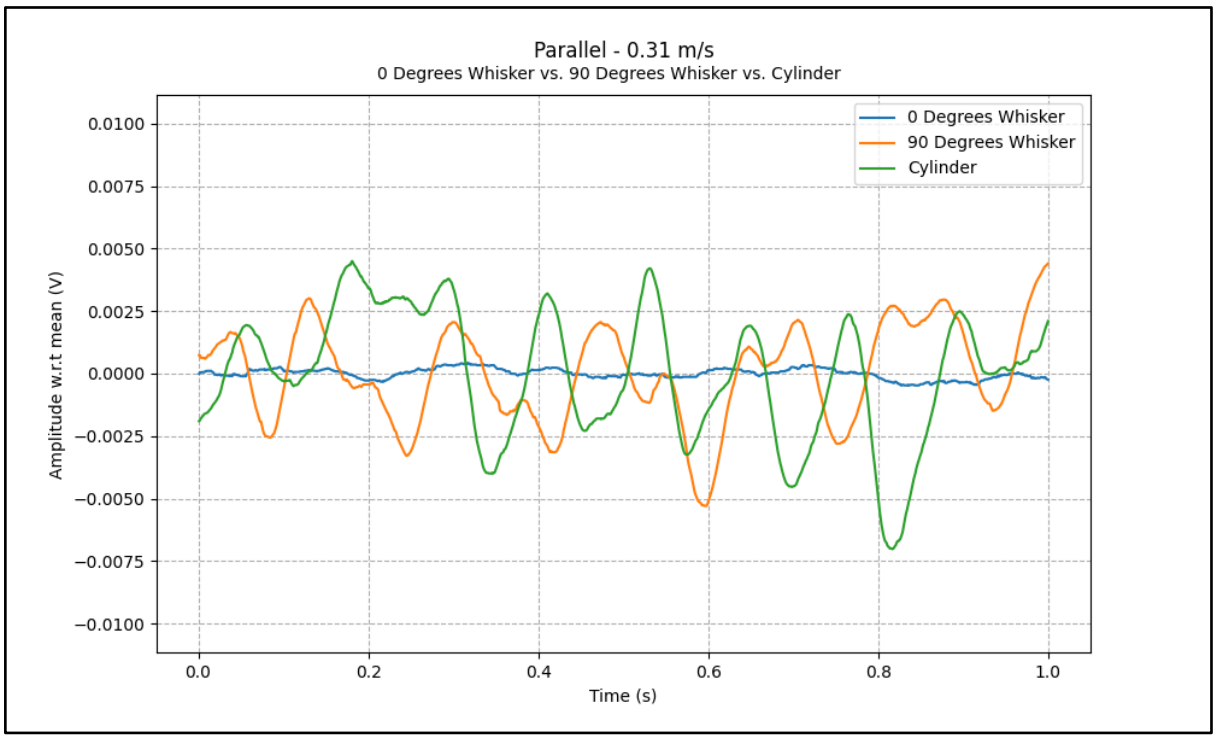

Figure A19: Graph of the (processed) sensor output versus time, as recorded by the sensor perpendicular to the flow, for a flow speed of 31 cm/s.

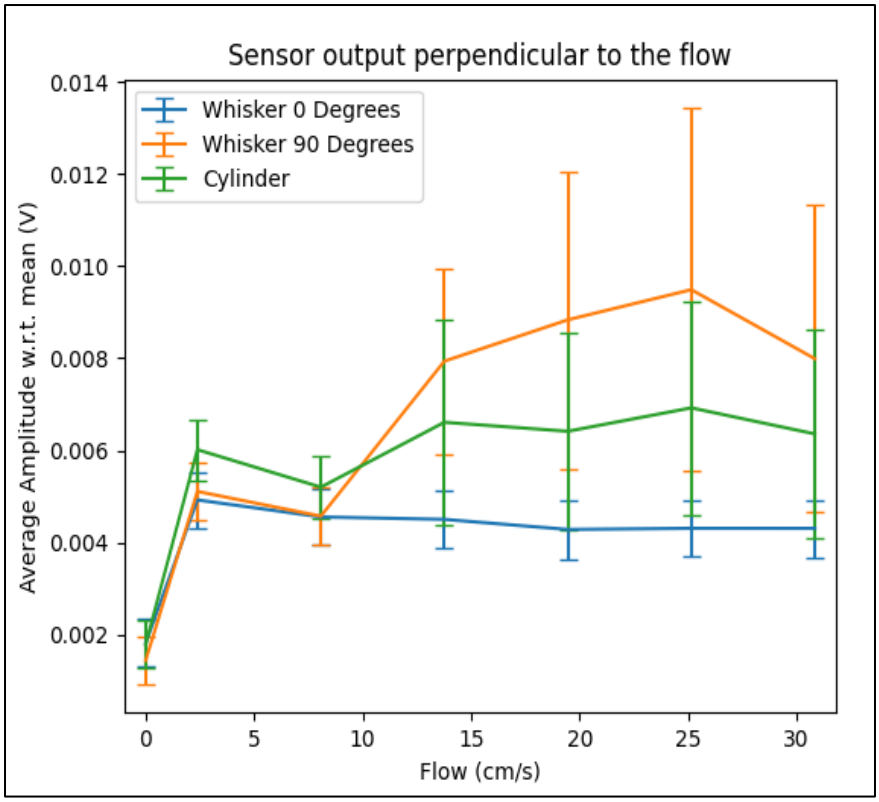

Figure A20: Graph displaying the averaged absolute maximal voltage output versus the flow speed, for the sensors perpendicular to the flow.

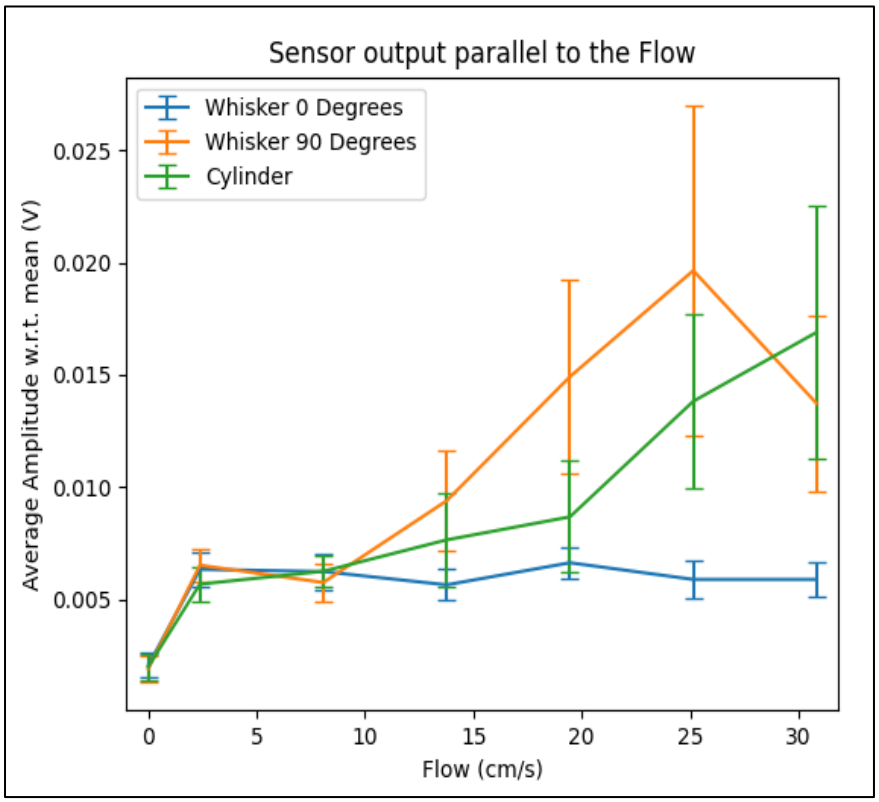

Figure A21: Graph displaying the averaged absolute maximal voltage output versus the flow speed, for the sensors parallel to the flow.

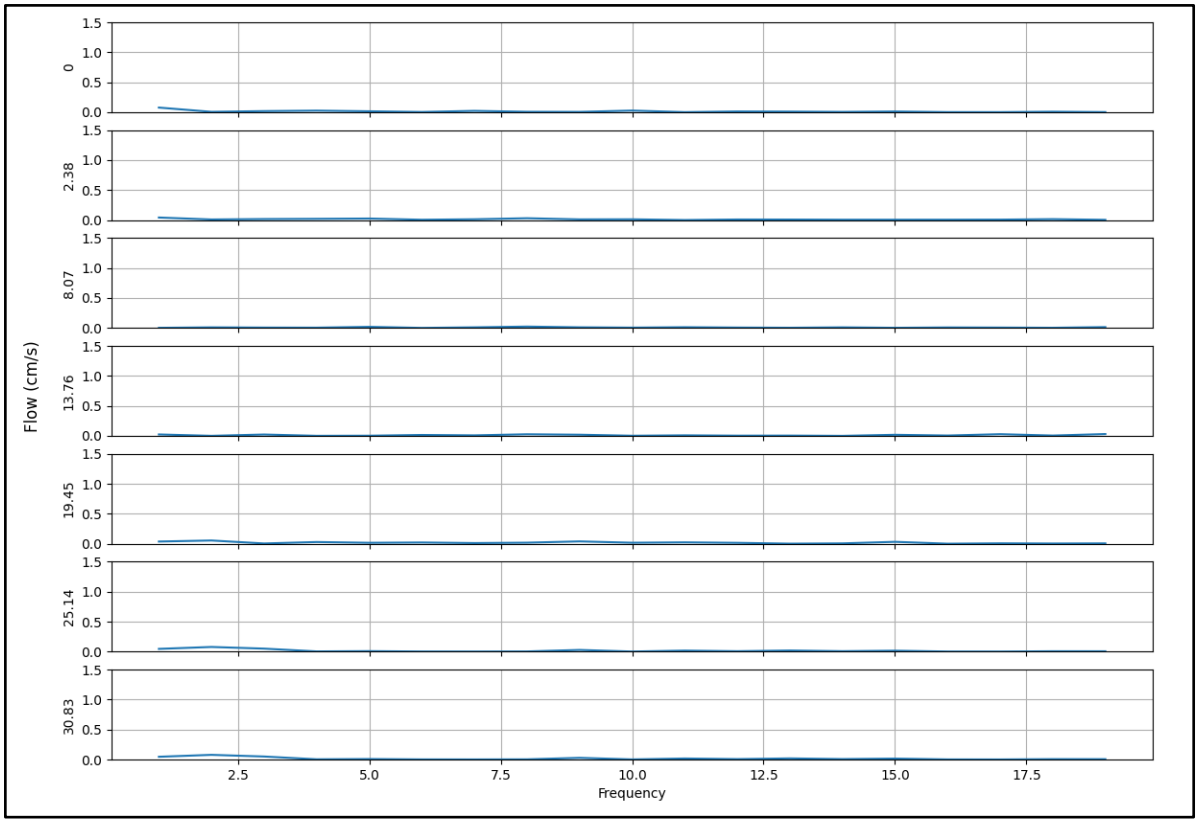

Figure A22: Graph of the frequency magnitude versus the frequency for 6 different flow speeds as measured by the sensor perpendicular to the flow for the whisker at a 0 degrees orientation.

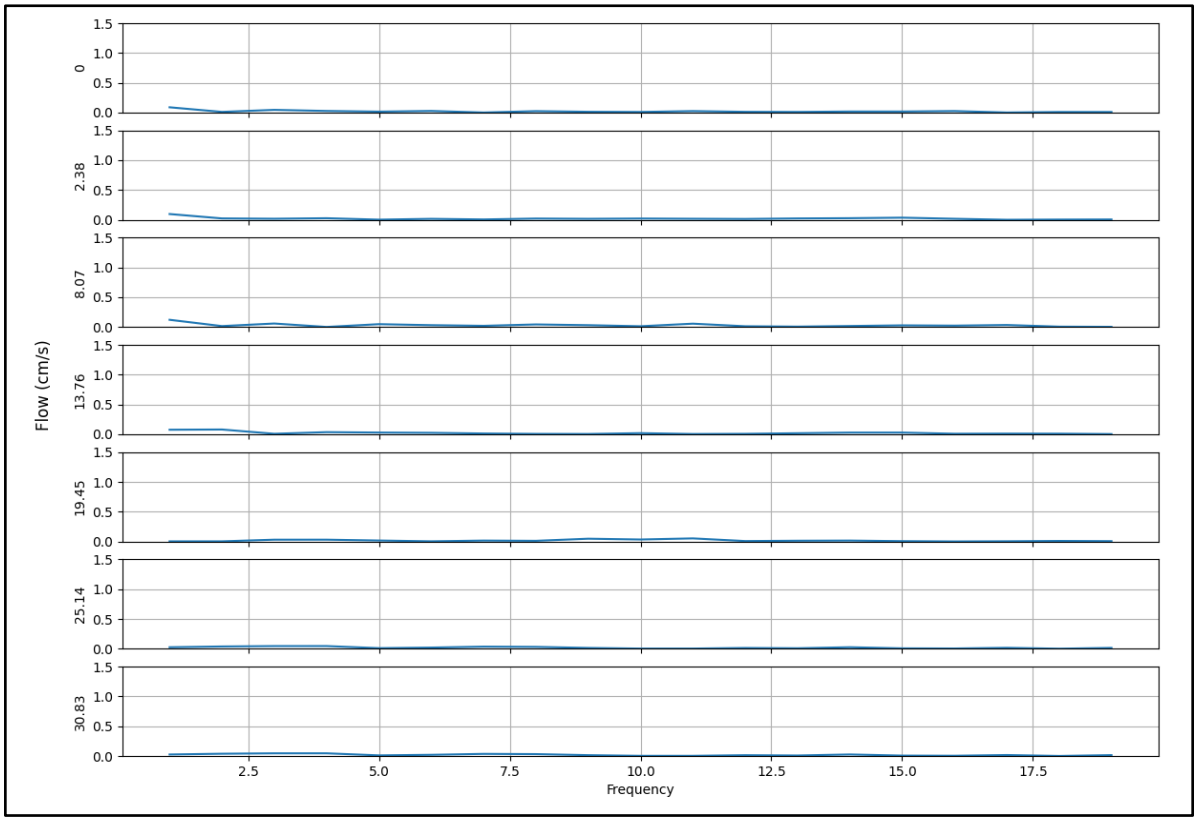

Figure A23: Graph of the frequency magnitude versus the frequency for 6 different flow speeds as measured by the sensor parallel to the flow for the whisker at a 0 degrees orientation.

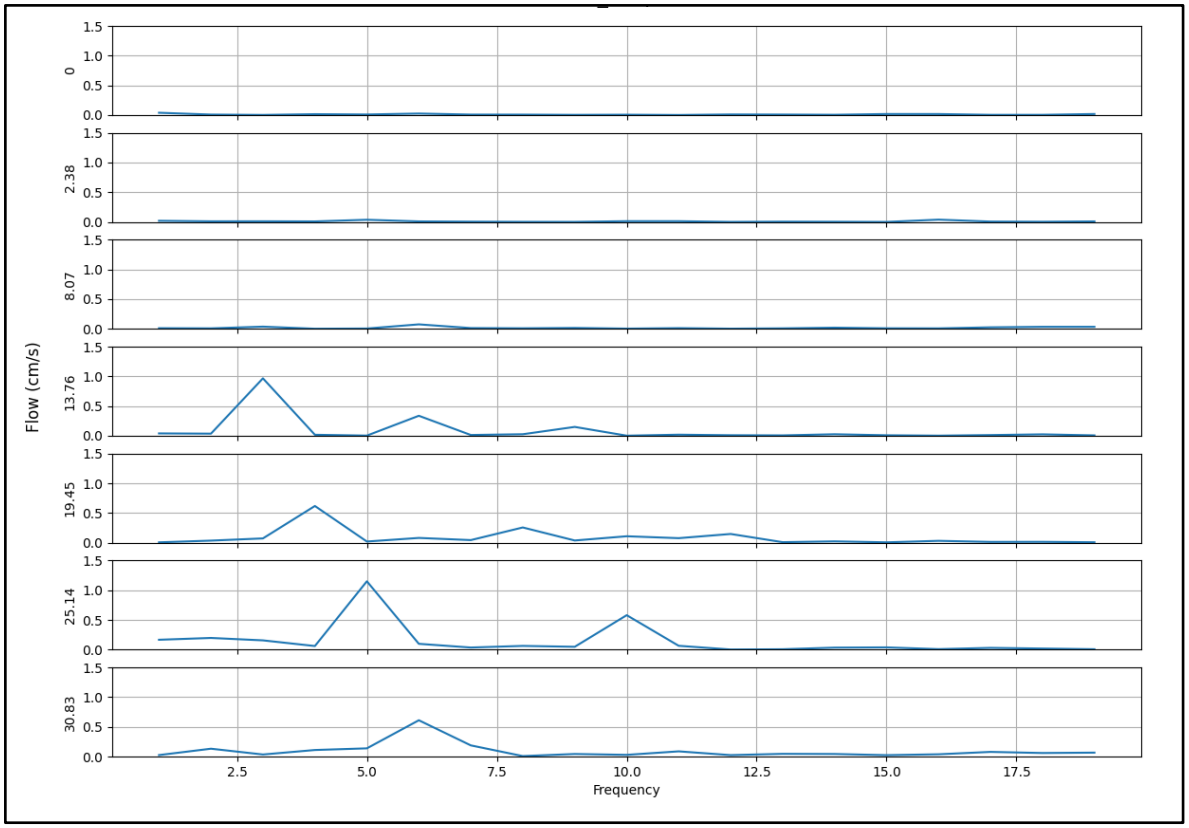

Figure A24: Graph of the frequency magnitude versus the frequency for 6 different flow speeds as measured by the sensor perpendicular to the flow for the whisker at a 90 degrees orientation.

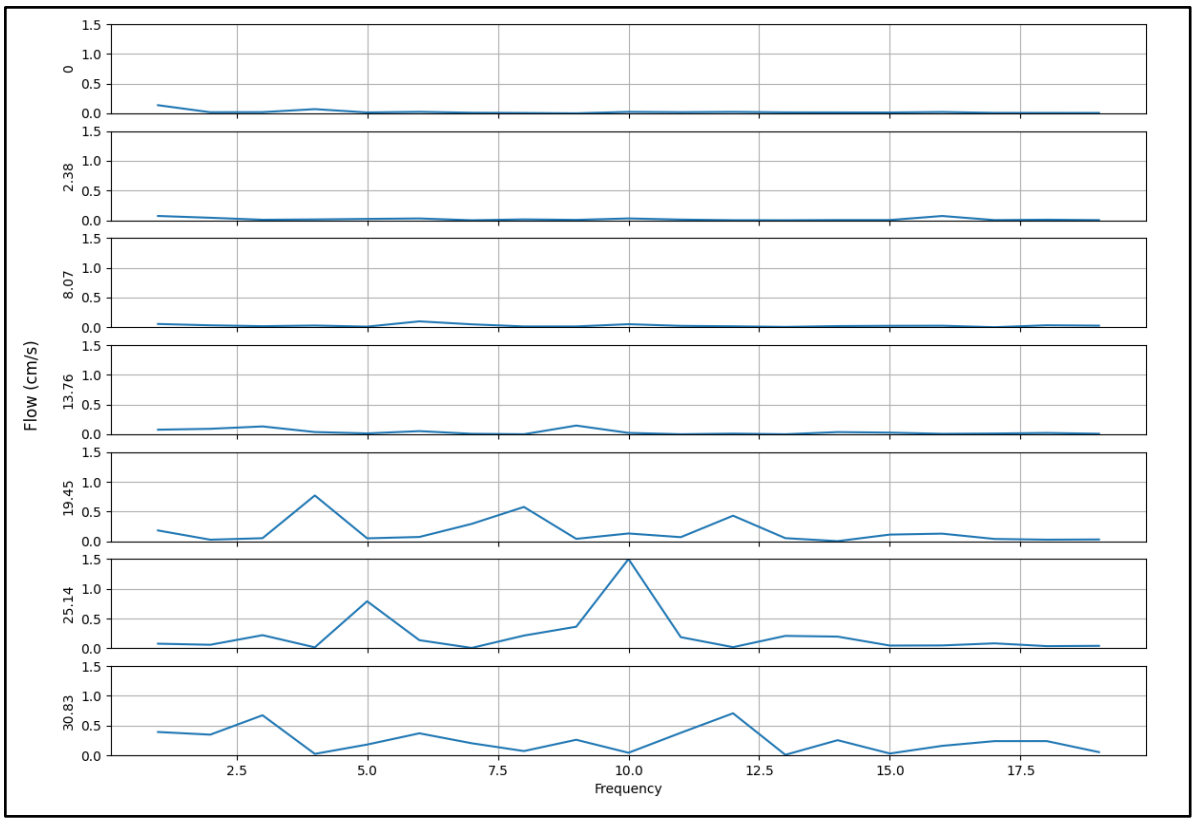

Figure A25: Graph of the frequency magnitude versus the frequency for 6 different flow speeds as measured by the sensor parallel to the flow for the whisker at a 90 degrees orientation.

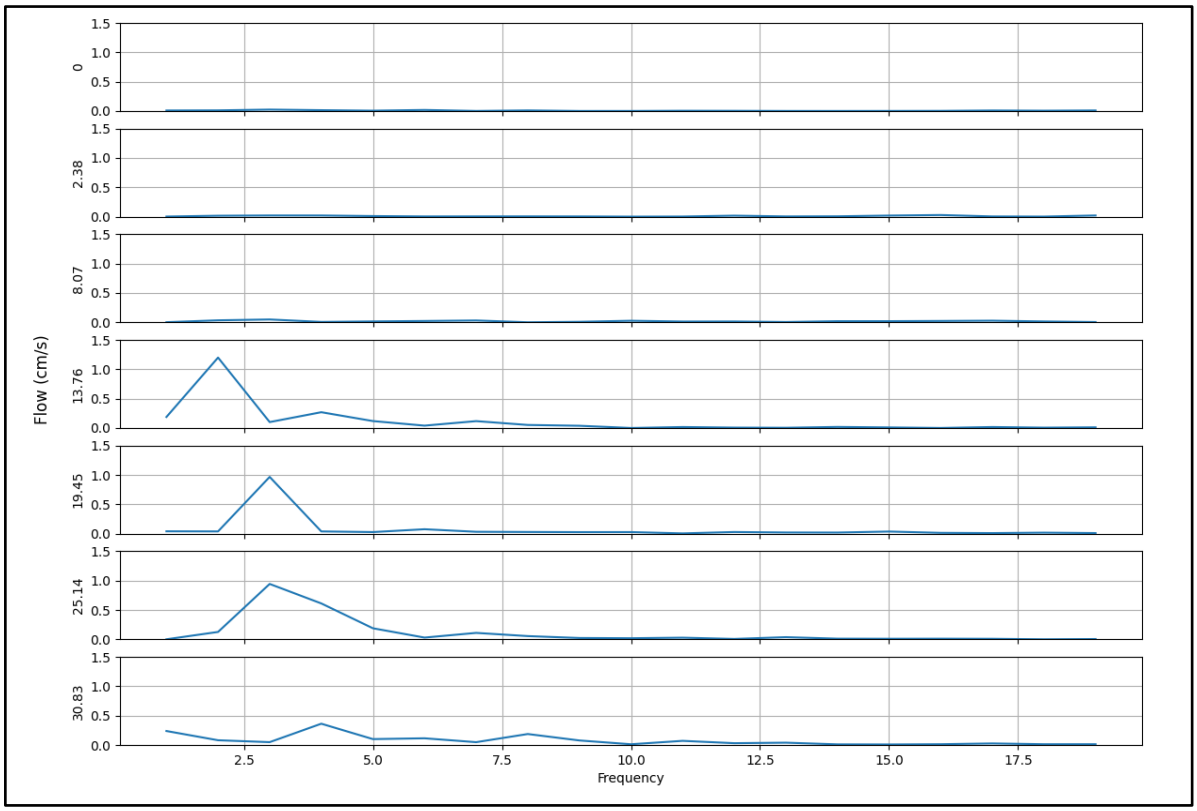

Figure A26: Graph of the frequency magnitude versus the frequency for 6 different flow speeds as measured by the sensor perpendicular to the flow for the cylindrical whisker.

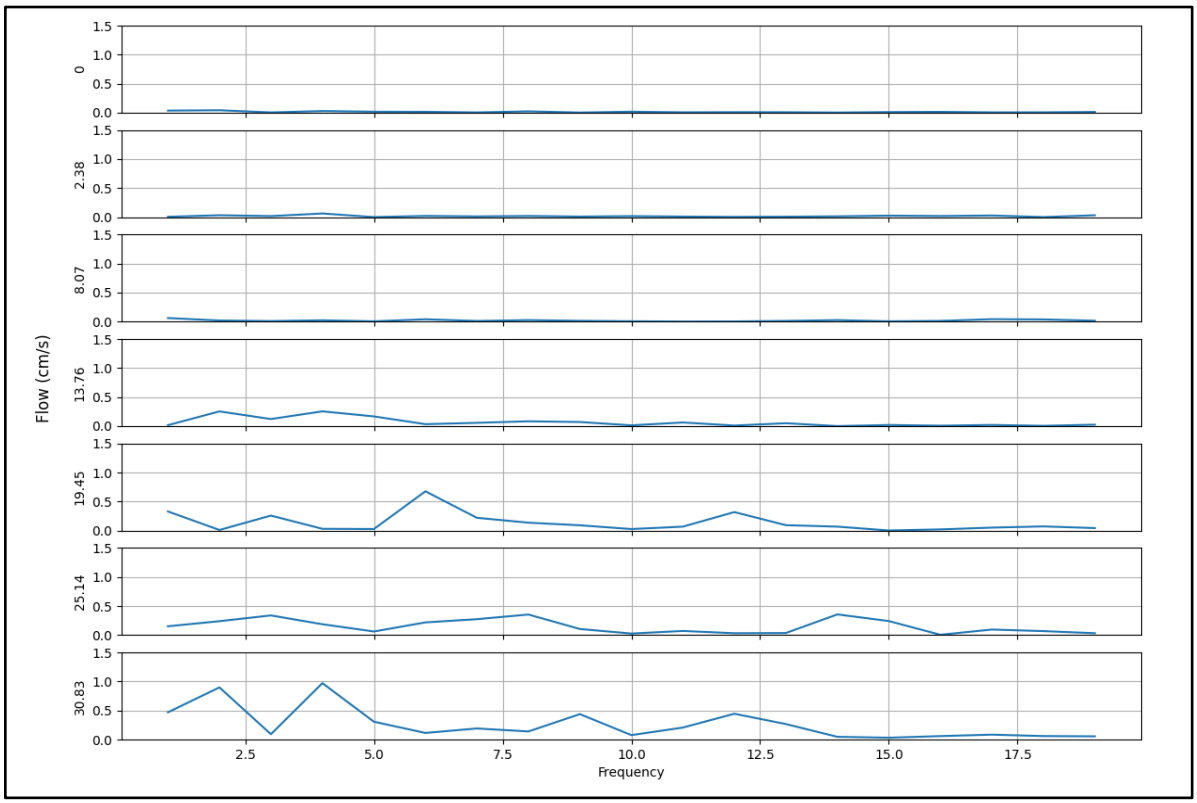

Figure A27: Graph of the frequency magnitude versus the frequency for 6 different flow speeds as measured by the sensor parallel to the flow for the cylindrical whisker.

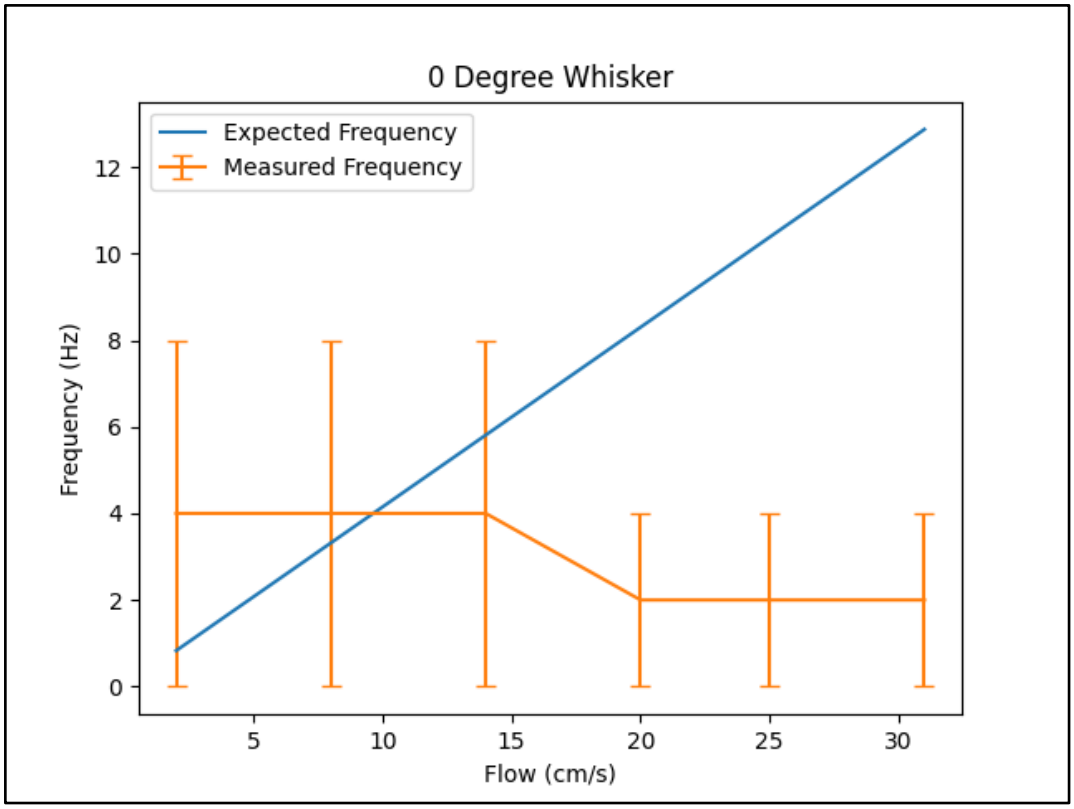

Figure A28: Graph of the expected and measured frequency at which the VIV are occurring for the whisker at a 0 degrees orientation.

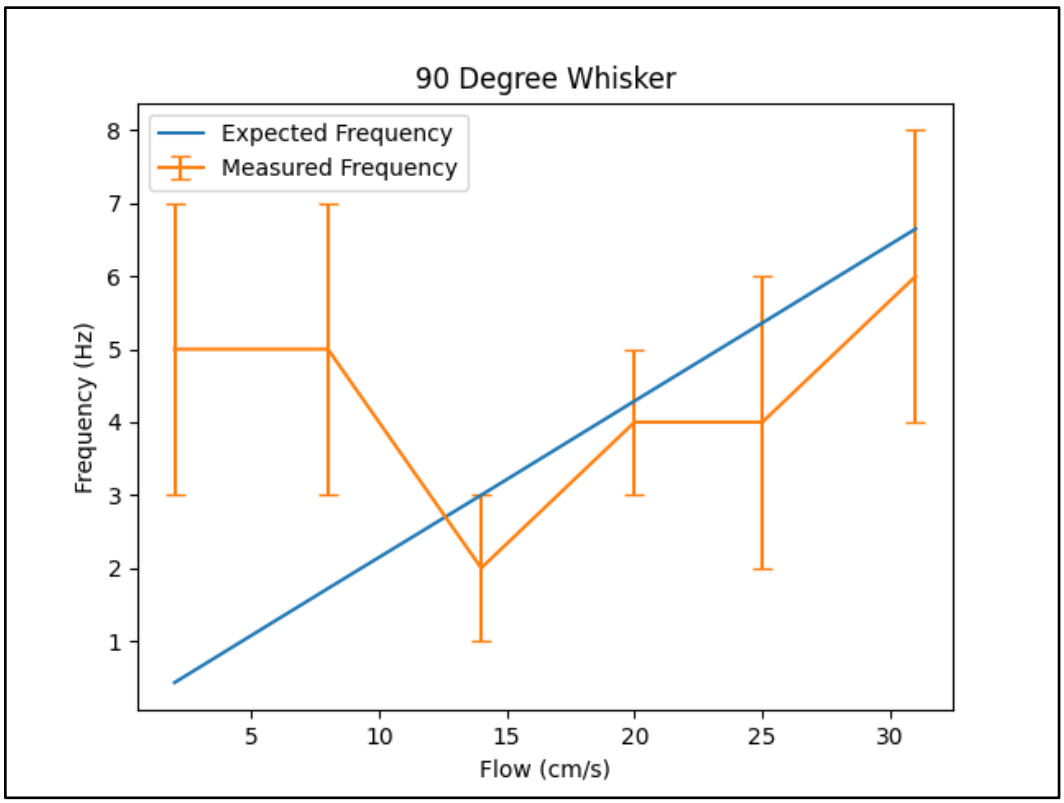

Figure A29: Graph of the expected and measured frequency at which the VIV are occurring for the whisker at a 90 degrees orientation.

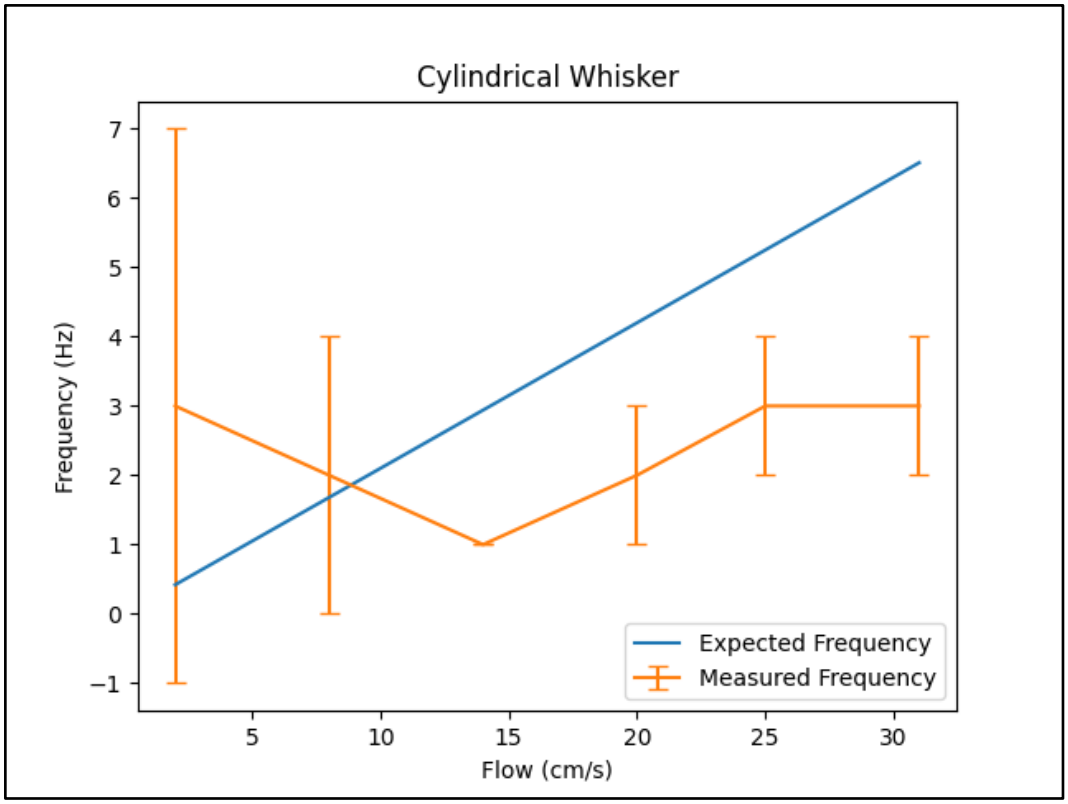

Figure A30: Graph of the expected and measured frequency at which the VIV are occurring for the whisker at a 90 degrees orientation.